STUDY OF BARIUM STRONTIUM TITANATE VARACTOR AT HIGH FREQUENCY

Cheng Weining

(B. Sc., University of Sci. and Tech. of China, P. R. China)

A THESIS SUBMITTED FOR THE DEGREE OF THE MASTER OF SCIENCE

DEPARTMENT OF PHYSICS

NATIONAL UNIVERSITY OF SINGAPORE

2007

ACKNOWLEDGEMENTS

Above all, I'd like to express my sincerest gratitude to my supervisor, Professor Ong Chong Kim for a lot of things he has done to help me in my research work. He showed me the labs in Physics Department in order to let me be familiar with the staff and facilities in the labs. He supported me in design and fabrication of the high frequency and low temperature measuring tube by assisting me in contacting workshop. This kind of help is of great useful to a freshman. He also create active and free academic atmosphere in our Centre for Superconducting and Magnetic Material (CSMM). In this circumstance, my knowledge has been enhanced and extended significantly and I have learned many skills which are helpful to my future work.

Secondly, I thank National University of Singapore (NUS) and Singapore Defense for the financial support to me and the project which I participate in these two years. Moreover, I give my thankfulness to the staffs in first year lab, third year lab, surface science lab and workshop that assisted me in doing my experiments and fabricating apparatus accessories.

Thirdly, my colleagues deserve to be thanked with my heart. During these two years of study, they have provided me a lot of help on data analysis and maintenance

of facilities. I am also extremely grateful to my colleagues in the lab who are working hard day in and day out to finish the project with me. I am sincerely thankful and appreciative for their efforts. Their passion and encouragement have helped me to maintain an optimistic attitude towards my experiment; never to give up. Here special thanks to Dr. Liu Huajun, Dr. Liu Yan, Dr. Ma Yungui, Dr. Tan Chin Yaw, Dr. Wang Peng, Dr. Yan Lei, Miss Lim Siew leng, Miss Phua Li Xian, Mr. Chen Xin, Mr. Ning Min, Mr. Zhang Gufei

Fourthly, I want to also express my thankfulness to Dr. Lin Guoqing and Dr. Kong Lingbing in Temasek Laboratories. They help me in making target for use in thin film deposition and they gave me a lot of guidance in this thesis.

Last but not least, I would like to thank my whole family. My wife, Ju Xiaoxiao undertook a lot of housework to free me in doing experiment and made life became colorful with many funs. My parents and my brother supported me from my home at China. Their encouragement and concern for me never stopped when I left home two years ago.

TABLE OF CONTENTS

SUMMARY

Ferroelectric materials have attracted great research interests due to their extraordinary electrical and electromechanical properties in the past few decades. A lot of application such as varactors, phase shifters, tunable filters are fabricated and studied. $Ba_xSr_{1-x}TiO_3$ is one of the promising ferroelectric materials to fabricate varactors due to its high dielectric constant, high tunability in an applied electric field (or bias) and low loss tangent. The composition x of Ba in the specimen determines the Curie temperature (or Curie point) at which $Ba_xSr_{1-x}TiO_3$ undergoes a phase change between paraelectric and ferroelectric.

In this thesis, $Ba_{0.5}Sr_{0.5}TiO_3$ (BST) which has a Curie temperature at room temperature is chosen to fabricate a room temperature varactor with low loss in high frequency. Varactor can be made as a planar structure, the co-called “planar capacitor” or as a parallel plate “sandwich” structure. In this work, parallel plate structure is used because relatively small dc voltages (1-20 V) are sufficient to achieve effective tuning. Pulsed laser deposition (PLD) was used as the main fabrication method to deposit the BST thin films and $La_{0.7}Sr_{0.3}MnO_3$ (LSMO) thin films. The Au thin films are deposited as electrodes by ion sputtering. Lithography and wet etching are conducted to pattern the top electrode.

We focused our research on investigating the correlation between the bottom electrode and the dielectric properties of the BST thin films. Three types of

$Ba_{0.5}Sr_{0.5}TiO_3$ (BST) thin film parallel plate varactor (BST/LSMO, BST/Pt and BST/Au) with different bottom electrodes are studied. The electrodes that are used are perovskite conducting oxide LSMO, Pt and Au. For the BST/LSMO varactor, a special study of deposition temperature effect on surface roughness of LSMO is studied in order to grow high quality BST thin film on the LSMO bottom electrode layer.

Dielectric constant and loss versus applied bias are characterized by impedance analyzer from 0 to 20 voltages. Dielectric constant and loss versus frequency under different applied bias are characterized in the frequency range from 200MHz to 10GHz by Vector Network Analyzer. The dielectric dispersion as a function of frequency is attributed to the increase of the effective separation length between top and bottom electrodes which is arising from the voltage drop across the bottom electrode in a varactor. The main source of the varactor loss is due to the resistance of bottom electrode. Varactors using Pt or Au as a bottom electrode have relatively small loss factor and frequency independent dielectric constant, and hence they are suitable to be used in a varactor for high frequency microwave application.

LIST OF TABLES

LIST OF FIGURES

LIST OF ABBREVIATIONS AND SYMBOLS

Spontaneous polarization	$\boldsymbol{P}_s$
Remnant polarization	$\boldsymbol{P}_r$
Eoercive field strength	E_c
Curie point	$\boldsymbol{\Theta}_c$
Angular frequency	ω
Atomic Force Microscopy	AFM
Centre for Superconducting and Magnetic Materials	CSMM
Frequency	$\boldsymbol{f}$
Prefix used to indicate an imaginary number	$\boldsymbol{j}$
LaAlO3	LAO
Pulsed Laser Deposition	PLD
Reflection S-parameter	S_{11}
Scanning Electron Microscopy	SEM
X-Ray Diffraction	XRD
Loss tangent	$\tan\delta$

CHAPTER ONE:

INTRODUCTION

1.1 Ferroelectric materials and applications

Ferroelectric materials have drawn a lot of attention for their excellent pyroelectric, piezoelectric, photorefractive, radiation-hard, acoustic and dielectric properties. The term ferroelectric is used in analogy to ferromagnetism, in which a material exhibits a permanent magnetic moment. Ferromagnetism was already known when ferroelectric was first discovered. Thus, the prefix "ferro", meaning iron, was used to indicate the property despite that fact that most ferroelectric materials do not have iron in their lattice. For some ferroelectrics, iron contaminants will reduce their long term reliability. Ferroelectric property materials was first found in 1921, in Rochelle salt single crystal (potassium sodium tartrate--KNa $(C_4H_4O_6)\cdot 4H_2O$). This crystal has very good piezoelectric properties and was used for many years before new ferroelectrics emerged. During the World War II, ferroelectric materials were fully developed and new material ($BaTiO_3$) with high permittivity was found. After this breakthrough, many applications and development have been made.

Piezoelectricity is the ability of some materials (notably crystals and certain ceramics) to generate an electric charge in response to applied mechanical stress. This property can be used in high voltage and power sources, sensors, miniature motor and etc.

Pyroelectricity is the ability of certain materials to generate an electrical

potential when they are heated or cooled. As a result of this change in temperature, positive and negative charges move to opposite ends through migration (i.e. the material becomes polarized) and hence, an electrical potential is established. Passive infrared sensors are often designed around pyroelectric materials, as the heat of a human or animal from several feet away is enough to generate a difference in charge.

The photorefractive effect is a nonlinear optical effect seen in certain crystals and other materials that respond to light by altering their refractive index. The effect can be used to store temporary, erasable holograms and is useful for holographic data storage. For example the material KH_2PO_4 (KDP), which is first reported by Busch and Scherrer in 1935[1], can be combined with a birefringent crystal to form an optical information storage and laser stochastic sweep displays.

The ferroelectric materials have high dielectric constant which can be used in semiconductor industry in fabricating the MOSFET device. This kind of materials is called high-k materials with the potential to replace silicon dioxide. Hysteresis in the "polarization versus electric field" property can be used to make ferroelectric RAM for computers and RFID cards. Ferroelectric RAM (FeRAM or FRAM) is a type of non-volatile computer memory. It is similar in construction to DRAM, which is currently used in the majority of a computer's main memory, but uses a ferroelectric layer to achieve non-volatility.

Beside the material and application mentioned above, a part of the most widely used and researched ferroelectric structural types, compositions, applications and their state of development are presented in Table 1. [2-9]

Structural Family	Composition	Application	Development Stage
Perovskite	$BaTiO_3$	capacitors	Commercialized
	$(Ba,Sr)TiO_3$	IR Detectors	Development
	$(Ba,Sr)TiO_3$ (doped)	PTCR Thermistors	Commercialization
	$Pb(Zr,Ti)O_3$ (PZT)	Transducers	Commercialization
	$Pb,La(Zr,Ti)O_3$(PLZT)	Actuators Electro-optics	Deve1opment Commercialization
	Ca-doped $PbTiO_3$	Transducers (hydrophones)	Development/ Commercialization
	Sm-doped $PbTiO_3$		
	$Pb(Sc,Ta)O_3$	IR Detectors	Development
	$(Na.Bi)TiO_3$	Transducers (Pb free)	Research
	$Pb(Mg,Nb)O_3$ (Relaxers)	Capacitors	Commercia1ization
		Actuators	development
		Electro-optics	Research
Tungsten-Bronze	$Ba(Zn,Ta)O_3$	Microwave Resonators	Commercialization
	$PbNbO_6$	Transducers (hydrophones)	Commercialization

	$(Sr,Ba)Nb_2O_6$	Electro-optics	Research/ Development
Bismuth-Layer Structure	$Bi_4Ti_3O_{12}$, Bi_2WO_6	Transducers (accelerometers)	Commercialization
Perovskite-Layer Structure	$Sr_2Nb_2O_7$	Transducers (high-temperature)	Research
	$La_2Ti_2O_7$		
	$Bi_2(Zn,Ni,Nb)O_2$	Capacitors	Development/ Commercialization
Composites	PZT/Polymer	Transducers	Development
Polymers	PVF2,Co-polymers	Transducers	Development/ Commercialization
Miscellaneous	$Li_2B_4O_7$ and $AlPO_4$ (Crystals)	Transducers (high frequency)	Development
	ZnO films		Commercialized
	AlN films		Research

Table 1.1 Ferroelectric Material and Applications [2]

Examples of applications in the field of microwave engineering include

field-dependent capacitors, tunable resonators, phase shifters, frequency-agile filters, variable power dividers and variable-frequency oscillators. Nonlinear applications such as harmonic generation, pulse shaping, mixing and parametric amplification are also a possibility. Such components have a wide range of applications in many communication and radar systems. For example, variable-phase shifters, one of the first and simplest components to be made with ferroelectrics, are used in antenna arrays in order to produce a beam scanning function. It is possible to integrate ferroelectric materials to produce complex electronically steerable antenna arrays with applications in both military and commercial radar and communication systems. Electronically controlled filters can be produced with applications of interference suppression, secure communications, dynamic channel allocation, signal jamming and satellite and ground-based communications switching. Many new systems concepts will appear as high-performance materials emerge, and these systems will have considerably improved performance over conventional systems.

1.2 Tunable thin film device

Due to various reasons related to both device electronics and materials technology, it is only in the past decade that intensive development efforts are being made in ferroelectric thin film [10, 11]. Ferroelectric thin films ($BaTiO_3$, $PbTiO_3$, PLZT, $KNbO_3$, $Sr_{1-x}Ba_xNb_2O_6$ and $Sr_{1-x}Ba_xTiO_3$) have been studied and developed rapidly since a few decades ago. There are several reasons for the increasing importance of ferroelectric thin films. First, the trend toward miniaturization of electronic components has led to the development of thin film ferroelectric devices performing

the same electronic functions, with only a fraction of the volume of the devices based on bulk ceramic or single crystal elements. Secondly, ferroelectric thin films are fast replacing the expensive single crystal ferroelectrics. Thin films have the additional designing advantages of a small volume and a large geometrical flexibility over single crystals. At last, new areas of application are being identified that utilize new device concepts, exploiting properties that are unique to both thin films and ferroelectric materials. For the thin film, the change in dielectric constant as a function of electric field is the key to a wide range of applications. Despite the large potential of this technology there have been few demonstrations of useful devices. There are a number of reasons for this [12]: (i) The large loss tangents of the practical ferroelectric materials result in low Q resonators and lossy delay lines. (ii) The large dielectric constants result in low impedance transmission lines and problems with surface wave modes. (iii) The design of complex bias networks is difficult. However, a number of microwave circuits have been produced. In 1987, ferroelectric nonvolatile memory integrated with silicon complementary metal-oxide semiconductor (CMOS) was demonstrated [13]. Another device is phase shifter. The phase shifter is by far the simplest component that can be produced by ferroelectric materials and hence it has been reported by a large number of laboratories. It simply consists of a ferroelectric transmission line of appropriate length. The transmission line must be matched to the external 50 Ω systems and have a low loss. It must also have large phase shifts, preferably of 360°, with low applied voltage. Depending on the application, the power requirements may be severe. A number of devices have been demonstrated based on

thin film technology [14, 15]. For the filters, despite frequency agile filters being of paramount importance in microwave systems, surprisingly few ferroelectric filters have been produced. Figure 1.1 shows three frequency-agile filters based on the use of ferroelectric thin films. Filters have been demonstrated with coplanar, microstrip and waveguide [16] technologies. Figure 1.1(a) shows layout of the three-stage HTS tunable filter with patterned ferroelectric thin film on $LaAlO_3$ single crystal substrate [17]. Figure 1.1(b) shows a bandstop filter based on a conventional transmission line coupled to a single crystal STO resonator with YBCO deposited on both sides [18]. Figure 1.1(c) shows the layout of a dual-spiral bandpass filter with a 633 MHz centre frequency and a 7% bandwidth [19].

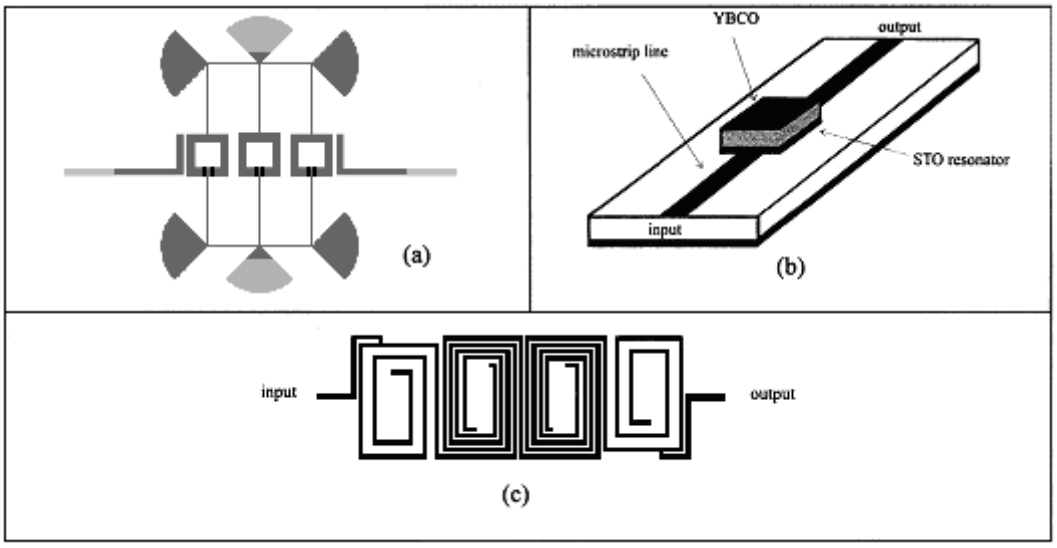

Figure 1.1 Three ferroelectric filters: (a) tunable thin-film filter [17]; (b) single-crystal STO bandstop filter [18]; (c) thin-film microstrip filter [19].

In the above discussion a dc or low-frequency bias has been assumed to be applied to the ferroelectric material in order to change its dielectric properties. However, ferroelectric materials respond very rapidly and can react to the microwave signal amplitude itself. The application of the microwave signal itself alters the

dielectric constant and therefore the propagation conditions of the signal; this nonlinear effect causes a distortion. For signals of small amplitude, this effect is small. But for large-amplitude signals this may be a significant problem. This nonlinear property of ferroelectrics can be used in principle for many devices, for example harmonic generators, parametric amplifiers, limiters, modulators and other nonlinear components. A harmonic generator using $Ba_xSr_{1-x}TiO_3$ was demonstrated as early as 1961 [20]. This generator operated at a fundamental frequency of 3 GHz with a conversion to 9 GHz using the ferroelectric material. An efficiency of 8.5% with an input power of 2.2 kW was obtained. Although much of the recent device work is not concerned with such high powers, the principle of operation of this generator is of interest to research of today.

1.3 The objective of the study

Being a special function electronic material, ferroelectric material has two basic properties: spontaneous polarization and reversibility under applied bias. Though there are over 200 kinds of ferroelectric material have been reported [21], potential candidate for integrated ferroelectric units is few. Unlike bulk material, thin film material has one more effect factor which is the relationship with substrate, bottom electrode, buffer layer and etc. The epitaxial growth of thin film is very important to the function of ferroelectric thin film.

$Ba_xSr_{1-x}TiO_3$ is one of the best perovskite structure candidates for applications because of its high dielectric constant and relative low loss. Different proportion of Ba and Sr of $Ba_xSr_{1-x}TiO_3$ has different Curie temperature where the $Ba_xSr_{1-x}TiO_3$

undergoes a phase transition between paraelectric and ferroelectric. $Ba_{0.5}Sr_{0.5}TiO_3$ (BST) has a Curie temperature near room temperature. Actually the ferroelectric devices we used are usually working under paraelectric phase. So BST is suitable for room temperature device study.

In our work, we study the effect of bottom electrode to the performance of varactor working in microwave frequency range. The quality of thin film structure and resistance are investigated. An explanation was given for the dielectric dispersion as a function of frequency.

A brief outline of this thesis is given as follows:

First, a brief introduction about this study, including applications, background information and our motivations, is given in Chapter 1. Systematical reviews about the basic understanding of ferroelectric material, theories of high frequency electromagnetism and previous investigations on BST for microwave applications are listed in Chapter 2. During this research, various measurements are required for the evaluation of BST varactor. Therefore, before the engagement of this investigation, Chapter 3 will be preceded with the introduction of experimental techniques used in this work, including the samples fabrication, characterization techniques and data analysis methods. Based on the review of previous investigations in Chapter 2, we design and fabricate BST/LSMO, BST/Pt and BST/Au varactors to study the relationship between bottom electrode and permittivity as well as loss tangent. Thus Chapter 4 will continually introduce the detailed fabrication process in this varactor study and the structure information.

Chapter 5 will systematically report the effect of bottom electrode on dielectric property of high frequency ferroelectric parallel plate varactor. Finally, the thesis is completed with Chapter 6, conclusion about the varactor dielectric properties under different bottom electrode.

References

[1] G. Busch and P. Scherrer, “Eine neue seignette-elektrische Substanz”, *Naturwissenschaften* **23**, 737 (1935)

[2] Thomas R. Shrout and Scott L. Swartz, “Precessing of Ferroelectric and Related Materials: A Review”, *Proceedings of the Eighth IEEE International Symposium on Volume*, **30**, 80 (1992);

[3] T. Shiosaki, “Recent Developments in Piezoelectric Materials,” *Ferroeletrics*, **91**, 39 (1989).

[4] S. L. Swartz, “Topics in Electronic Ceramics,” *IEEE Trans. Elect. Insul. Dieest on Dielectrics* **25**, 935 (1990).

[5] L. L. Hench and J. K. West (Eds.), “Princinles of Electronic Ceramics”, John Wiley & Sons, Inc., New York, 1990.

[6] J. M. Herbert, “Ferroelectric Transducers and Sensors”, Gordon and Breach Science Publishers, Inc., New York (1982).

[7] G.H. Haertling, “Piezoelectric and Electro-optic Ceramics, in Ceramic Materials for Electronics: Processing, Properties, and Applications”, ed. by R. C. Buchanan, Marcel-Dekker, Inc., New York, pp. 139-225 (1986).

[8] R.C. Pohanka, P. L. Smith, and G.H. Haertling, “Recent Advances in Piezoelectric Ceramics, in Electronic Ceramics: Properties, Devices, and Applications”, ed. by L.M. Levinson, Marcel-Dekker, Inc., New York, pp**.** 45-145 (1988).

[9] Helmut Thomann, “Piezoelectric Ceramics,” *Advanced Materials*, **2**, 458 (1990).

[10] N. Setter, D. Damjanovic, H. Kohlstedt, etc, *Journal of Applied Physics*, **100**, 051606 (2006)

[11] A. K. Tagantsev, V. O. Sherman, K. F. Astafiev, J. Venkatesh and N. Setter, *Journal of Electroceramics*, **11**, 5 (2003)

[12] M. J. Lancaster, J. Powell and A. Porch, “Thin-film ferroelectric microwave devices”, *Superconductor Science and Technology* **11**, 1323 (1998)

[13] S. S. Eaton, D. B. Butler, M. Parris, D. Wilson, and H. McNeillie, “A Ferroelectric Nonvolatile Memory”, *Dig. Tech. Pap.-IEEE Int. Solid-State Circuits Conf.* **329**, 130 (1988)

[14] Jackson C. M., Pham T., Zhang Z., Lee A. and Pettiete-Hall C., "Model for a novel CPW phase shifter", *IEEE MTT-S Int. Microwave Symp.* 1439 (1995)

[15] De Flaviis F., Alexopoulos N. G. and Stafsudd O. M., "Planar microwave integrated phase-shifter design with high purity ferroelectric material", *IEEE Trans. Microwave Theory Tech.* **45**, 963 (1997)

[16] Kozyrev A. *et al*, "Ferroelectric films: nonlinear properties and applications in microwave devices", *IEEE MTT-S IMS Digest*, 985 (1998)

[17] C. Y. Tan and C. K. Ong, "Planar tunable HTS microwave filter with patterned ferroelectric thin film", *Superconductor Science & Technology*, **19**, 212 (2006)

[18] Gevorgian S, Carlson E, Kollberg E and Wikborg E., "Tunable superconducting bandstop filters", *IEEE MTT-S Digest*, 1027 (1998)

[19] C. K. Ong, Linfeng Chen, Jian Lu, C. Y. Tan, and B. T. G. Tan, "High-Temperature Superconducting Bandpass Spiral Filter", *IEEE Microwave and Guided Wave Letter*, **9,** 407 (1999)

[20] Didomenico M., Johnson D. and Pantell R., "Ferroelectric harmonic generator and large-signal microwave characteristics of a ferroelectric ceramic", *J. Appl. Phys.* **33**, 1697 (1962)

[21] 钟维烈.铁电物理学.北京：科学出版社，1996

CHAPTER 2:

LITERATURE REVIEW

2.1 Theory of ferroelectrics

The reason why ferroelectric materials have so many outstanding properties would be found out from its crystal structure. Fundamentally speaking, the nature of the ferroelectric property is caused by crystal spontaneous polarization. Spontaneous polarization is defined by the value of the dipole moment per unit volume, or by the value of the charge per unit area on the surface perpendicular to the axis of spontaneous polarization. For example, Figure 2.1 shows the crystal structure of the ferroelectric material $BaTiO_3$. Above the Curie temperature, the prototype crystal structure is cubic. Below the Curie temperature, the centre of cubic move up or down to form a polarization.

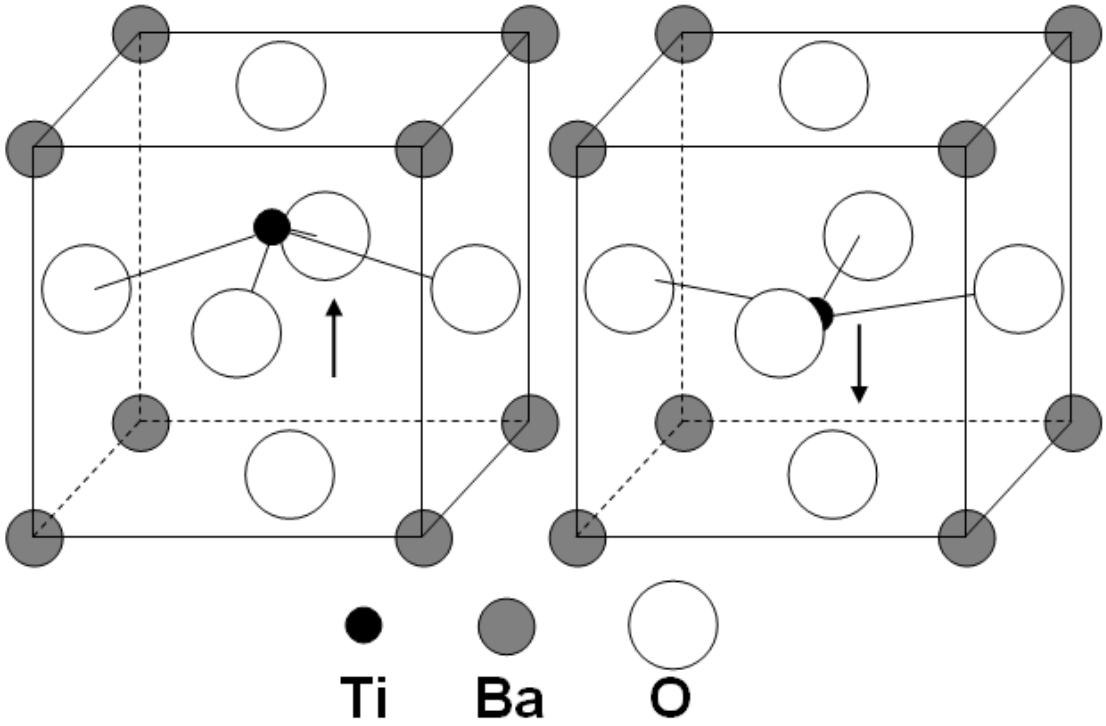

Figure 2.1 The crystal structure of perovskite-type $BaTiO_3$ material. Below the Curie temperature, there is a spontaneous polarization due to the bias of cubic centre.

In physics, the ferroelectric effect is an electrical phenomenon whereby certain materials may exhibit a spontaneous dipole moment, the direction of which can be switched between equivalent states by the application of an external electric field. Since electrical properties are strongly correlated with the crystal structure, the axis of spontaneous polarization is usually a crystal axis.

Although a crystal with polar axes exhibits piezoelectric effect, it does not necessarily have a spontaneous polarization vector, because the net result of electric moment along all polar axes may be equal to zero. Therefore, only a crystal with a unique polar axis exhibits a spontaneous polarization vector $\boldsymbol{P}_s$ along this axis. In general, this spontaneous polarization cannot directly be measured from the charges on the surfaces of the crystal, because these charges are compensated by external and/or internal carriers carrying an electric current, or by charges on the boundaries of twins. The value of the spontaneous polarization $\boldsymbol{P}_s$ depends on temperature. As temperature changes, a variation of the charge density can be observed on those surfaces of the sample which are perpendicular to the unique polar axis in a crystal without twins, or in a poled poly-crystal (ceramic) with oriented grains. This is the pyroelectricity in crystals exhibiting spontaneous polarization. Most pyroelectric crystals exhibit a spontaneous polarization $\boldsymbol{P}_s$ in a certain temperature range and the direction of $\boldsymbol{P}_s$ can be reversed by an external electric field. Such crystals are called ferroelectric crystals. Ferroelectricity was discovered as recently as 1921 by Valasck in Rochelle salt. From a physical point of view, ferroelectric crystals are those crystals which possess one or more ferroelectric phases. The ferroelectric phase is a

particular state exhibiting spontaneous polarization which can be reoriented by an external field. A reversal of polarization is considered as a special case of the polarization reorientation. In general, uniform alignment of electric dipoles only occurs in certain regions of a crystal, while in other regions of the crystal spontaneous polarization may be in the reverse direction (such as in twinning). Such regions with uniform polarization are called ferroelectric domains. The interface between two domains is called the domain wall. The ferroelectric domains were first demonstrated in a study of spontaneous birefringence [1, 2].

Another important characteristic of ferroelectrics is the ferroelectric hysteresis loop. The polarization P is a double-valued function of the applied electric field E. A ferroelectric hysteresis loop can be observed by means of a Sawyer-Tower circuit [3]. Firstly, the sample is applied with a small electric field, there is only a linear relationship between P and E, because the field is not large enough to switch any domain and the crystal will behave as a normal dielectric material (paraelectric). This case corresponds to the segment OA of the curves in Figure 2.2.

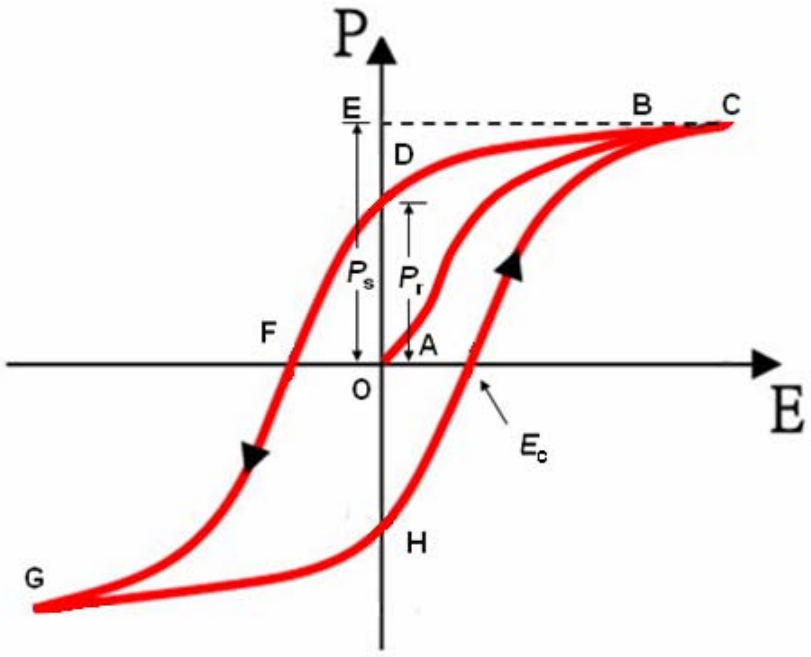

Figure 2.2 A typical P-E hysteresis loop in ferroelectrics

As the electric field strength increases, a number of the negative domains (which have a polarization opposite to the direction of the field) will be switched over in the positive direction (along the field direction) and the polarization will increase rapidly (segment AB) until all the domains are aligned in the positive direction (segment BC). This is a state of saturation in which the crystal is composed of just a single domain. As the field strength decreases, the polarization will generally decrease (at the point D in the figure) but does not return back to zero. When the field is reduced to zero, some of the domains will remain aligned in the positive direction and the crystal will exhibit a remnant polarization $\boldsymbol{P}_r$. The extrapolation of the linear segment BC of the curve back to the polarization axis (at the point E on the vertical axis in Figure 2.2) represents the value of the spontaneous polarization $\boldsymbol{P}_s$. The remnant polarization $\boldsymbol{P}_r$ in a crystal cannot be removed until the applied field in the opposite (negative) direction reaches a certain value (at the point F in the figure) The strength

of the field required to reduce the polarization P to zero is called the coercive field strength E_c. Further, increase of the field in the negative direction will cause a compete alignment of the dipoles in this direction and the cycle can be completed by reversing the field direction once again. Thus the relation between P and E is represented by a hysteresis loop (CDFGHC) as shown in Figure 2.2. Recent years' study shows that the there is anisotropy effect in the hysteresis loop, especially in thin film structure. The anisotropy is caused by the stress imposed by substrate or interface effect. Interdigital electrode and parallel plate electrode are often used to measure the microwave properties. The former method measures mainly in-plane dielectric properties while the later one measures the out-plane properties. The result could be different by these two methods if the sample is dielectric anisotropy.

Placing a ferroelectric material between two conductive plates creates a ferroelectric capacitor. Ferroelectric capacitors exhibit nonlinear properties and usually have very high dielectric constants. The fact that the internal electric dipoles can be forced to change their direction by the application of an external voltage gives rise to hysteresis in the "polarization versus voltage" property of the capacitor. In this case, polarization is defined as the total charge stored on the plates of the capacitor divided by the area of the plates.

Temperature of phase transition so called Curie point $\boldsymbol{\Theta}_c$ is another important characteristic of ferroelectrics. When the temperature decreases through the Curie point, a ferroelectric crystal undergoes a structural phase transition from a paraelectric phase to a ferroelectric phase. It's generally believed that the

ferroelectric structure of a crystal is created by a small distortion of the paraelectric structure such that the lattice symmetry in the ferroelectric phase is always lower than that in the paraelectric phase. When the temperature is in the vicinity of the Curie point, thermodynamic properties (such as dielectric, elastic, optical, and thermal properties) of a ferroelectric crystal show anomalies and the structure of the crystal changes. For example, the dielectric constant in most ferroelectric crystals has a very large value near their Curie points. This phenomenon is usually called the dielectric anomaly.

2.2 Measurement of dielectric properties in microwave frequency

To measure the dielectric properties of ferroelectrics at microwave frequencies, the ferroelectric thin film under test is usually fabricated into microwave device, and the dielectric properties of the thin film are derived from the device properties. These devices are discussed briefly below.

In a transmission line method, the thin film sample is usually fabricated into a coplanar waveguide. The ε_r and tanδ of the thin film are derived from the phase and amplitude of the transmission coefficient of the coplanar waveguide. Two approaches are often used to apply the dc bias voltages. One approach is to apply the bias voltage across the two ground planes of the coplanar circuit [4]. In this approach, the two ground planes are dc isolated from each other. The disadvantage of this approach is that it is difficult to achieve good grounding for the transmission line. Another approach is to apply the bias voltage to the signal trace of the coplanar waveguide. In this case, bias tees are often used to isolate the microwave instruments and the dc bias

voltage source. The advantages of coplanar waveguide method are that it only requires one layer of metallization and its wide measurement frequency range; however its accuracy and sensitivity are usually not very high.

In the resonator method, the ferroelectric thin film under study is usually fabricated into a coplanar resonator. The ε_r and tanδ of the ferroelectric film are deduced from the resonant frequency and Q factor of the coplanar resonator. The bias voltage can be directly applied to the resonator through the electric field node of the resonator or/and an rf choke. Resonator methods usually have higher accuracy and sensitivity, but measurements can only be conducted for a single or several discrete frequencies, i.e. at the fundamental and harmonic resonant frequencies.

In the capacitor method, the ferroelectric thin film is fabricated into a capacitor, and the ε_r and tanδ of the thin film are derived from the capacitance and Q factor of the capacitor.

The capacitance and Q factor of a capacitor at radio frequency and microwave frequencies are often measured by integrating the capacitor into a transmission line or a resonant structure. If the capacitor is integrated into a transmission line, the capacitance and Q factor of the capacitor can be derived from the phase and amplitude of the transmission coefficient through the transmission line. If the capacitor is integrated into a resonant structure, the capacitance and Q factor of the capacitor can be deduced from the resonant frequency and Q factor of the resonant structure. The dc bias voltage is often applied between the two electrodes of the capacitor.

The planar circuit methods are usually destructive in the sense that metallization

has to be coated on the ferroelectric thin film. Having a non-destructive testing method is desirable for device fabrication as it allows the confirmation of the thin film properties before committing the resources to fabricate it into a device.

2.3 Varactor Design

Two different types of varactors, planar (interdigital) [5, 6] or parallel-plate [7], are possible using BST thin films. The cross section sketch is similar with figure 2.3.

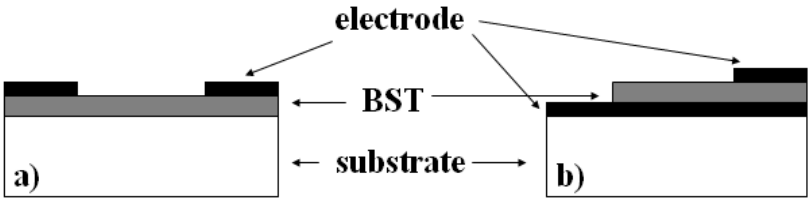

Figure 2.3 a) Planar and b) parallel-plate capacitors based on BST film. Notice that the bottom electrode was partly uncovered in b).

For the interdigital capacitors, BST films are directly deposited on the appropriate substrate followed by top interdigital electrode metallization. In general, interdigital devices are simpler to fabricate and integrate into circuits, but suffer from reduced tunability (due to large fringing electric field in the air) and higher control voltages. Having smaller spacing between the fingers can further increase available tunability at lower voltages, but requires more accurate fabricating technology. Typical operating voltages for interdigital capacitors are in the range of hundreds voltage. The parallel plate capacitors, on the other hand, can be operated with much lower bias voltages, making them attractive for most microwave and millimeter-wave applications [8]. For parallel plate capacitors, BST films are deposited directly on a bottom electrode on substrate. Then the top electrodes are defined creating metal-insulator-metal (MIM) structures. The distance between the electrodes is basically the BST film thickness

and much shorter than the spacing in the interdigital structures. That's why the control voltages typically scale with the film thickness. Also tri-layer structures offer a higher tunability compared to interdigital structures since the electric fields are better confined in the film. The control voltage or power handling capacity is easily manipulated through control of the material thickness, but the integration of bottom electrodes and other structures require more detailed fabrication. Figure 2.4 shows tunability curves for typical BST parallel plate structures. Since higher tunability can be obtained at relatively much lower bias voltages, the parallel plate capacitors offer more flexibility in many circuit applications.

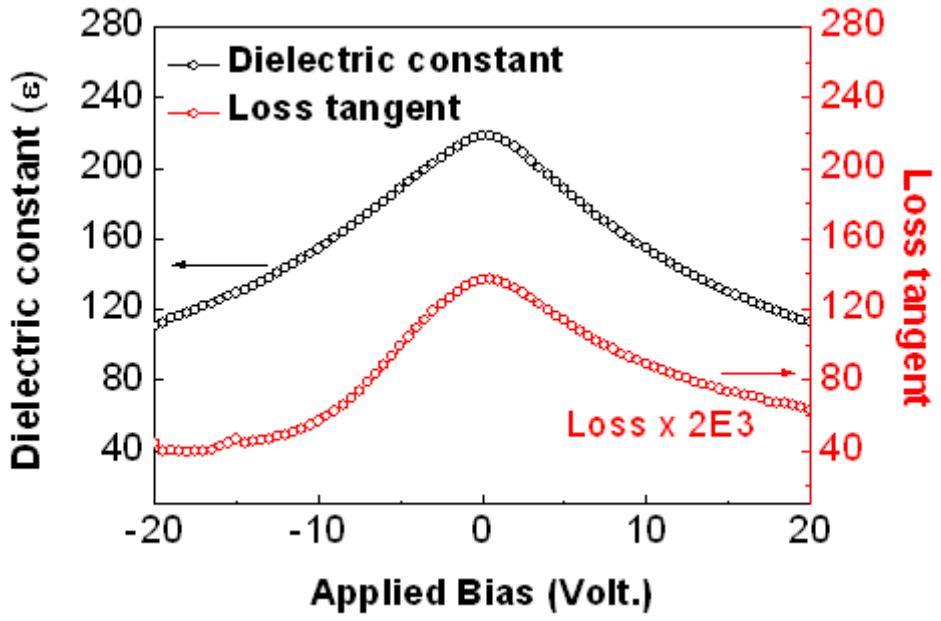

Figure 2.4 Field dependence of the dielectric constant and loss tangent of BST, characterized by impedance analyzer.

Silicon and $LaAlO_3$ (LAO) single crystal are carefully chosen as the substrate for the following thin film deposition. Silicon and LAO has a low loss tangent making it suitable for microwave applications. Also large area silicon substrates are available at

relatively low cost.

The temperature requirement to deposit the BST films in an oxygen environment is typically in the range of 600-800 ºC, making the bottom electrode choice crucial. Most integration schemes for perovskite dielectrics use noble metal or metal-oxide electrodes in combination with a deposited diffusion barrier material at the electrode/plug interface for DRAM applications [9]. High conductivity metals, such as Pt [10], Cu [11] and Au [12] have been considered. In this work, LSMO, Pt and Au are used as bottom electrode. Sputtering of Pt and Au are available in Department of Physics at National University of Singapore. LSMO has similar lattice parameters with BST we are going to study. So we expect high quality epitaxial BST layer on LSMO. Besides, LSMO is commonly used in Centre for Superconducting and Magnetic Material lab. A mature deposition procedure has already been developed.

One of difficulty involves adhesion of the Au electrode to the substrate, sometimes leading to process-induced delamination or hillock. Special care must be taken for the development adhesion layers to solve this problem.

Lithography is the key facility to pattern the top electrode. Since the minimum capacitance required, the size of the top electrode is in micron scale. Lithography is necessary for accurate fabrication and alignment. In this work, positive photoresist and soft mark bought from Innovative Laser Systems Inc. are used in lithography process.

References

[1] H. Blattner, W. Kanzig, W. J. Merz and H. Sutter, *Helv. Phys. Acta* **21**, 207 (1948).

[2] B. Batthias and A. von Hippel, "Domain Structure and Dielectric Response of Barium Titanate Single Crystals", *Phys. Rev.* **73**, 1378 (1948).

[3] C. B. Sawyer and C. H. Tower, "Rochelle Salt as a Dielectric", *Phys. Rev.* **35**, 269 (1930).

[4] M. J. Lancaster, J. Powell, and A. Porch, "Thin-film ferroelectric microwave devices", *Superconductor Science & Technology*, **11**, 1323 (1998).

[5] A. Vorobiev, P. Rundqvist, K. Khamchane, and S. Gevorgian, "Silicon substrate integrated high Q-factor parallel-plate ferroelectric varactors for microwave/millimeterwave applications", *Appl. Phys. Lett.* **83**, 3144 (2003).

[6] C. Y. Tan, L. F. Chen, K. B. Chong, and C. K. Ong, "Nondestructive microwave permittivity characterization of ferroelectric thin film using microstrip dual resonator", *Review of Scientific Instruments* **75**, 136 (2004);

[7] S. Gevorgian, T. Martinsson, P. L. J. Linner, and E. L. Kollberg, "CAD models for multilayered substrate interdigital capacitors", *IEEE Trans. Microw. Theory Tech.* **44**, 896 (1996);

[8] B. Acikel, L. Yu, A. S. Nagra, T. R. Taylor, P. J. Hansen, J. S. Speck, and R. A. York, "Phase shifters using (Ba,Sr)TiO/sub 3/ thin films on sapphire and glass substrates," *Microwave Symposium Digest, 2001 IEEE MTT-S International* **2**, 1191 (2001).

[9] B. E. Gnade, S. R. Summerfelt, and D. Crenshaw, "Processing and device issues of high permittivity materials for DRAMs", *Science and Technology of Electroceramic Thin Films*, NATA ASI Series, 373 (1995).

[10] D. E. Kotecki, J. D. Baniecki, H. Shen, R. B. Laibowitz, K. L. Saenger, J. J. Lian, T. M. Shaw, S. D. Athavale, C. Cabral, Jr., P. R. Duncombe, M. Gutsche, G. Kunkel, Y. J. Park, Y. Y. Wang, and R. Wise, "$(Ba,Sr)TiO_3$ dielectrics for future stacked capacitor DRAM", *IBM Journal of Research and Development*, **43**, 367 (1999).

[11] W. Fan, S. Saha, J. A. Carlisle, O. Auciello, R. P. H. Chang, and R. Ramesh, "Layered Cu-based electrode for high-dielectric constant oxide thin film-based devices", *Appl. Phys. Lett.* **82**, 1452 (2003).

[12] B. Acilel, T. R. Taylor, P. J. Hansen, J. S. Speck and R.A. York, “A new high performance phase shifter using $Ba_xSr_{1-x}TiO_3$ thin films”, *IEEE Microwave Comp. Lett.* **12**, 237 (2002).

CHAPTER 3:

EXPERIMENTAL TECHNIQUES

3.1 Pulsed laser deposition

There are several options for fabricating ferroelectric films, such as pulsed laser deposition, sputtering, screen printing, sol-gel and metal-organic chemical vapor deposition (MOCVD) [1-7]. The deposition techniques used in this thesis are pulsed laser deposition (PLD) and ion sputtering.

Pulsed laser deposition (PLD) is a thin film deposition which is one of a physical vapor deposition (PVD) technique. This deposition method uses a high power pulse laser beam is focused inside a vacuum chamber to strike on a target of the desired composition. Material is then vaporized from the target and deposited as a thin film on a substrate, such as a silicon wafer facing the target. This process can occur in ultra high vacuum or in the presence of a background gas, such as oxygen which is commonly used when depositing oxides to fully oxidize the deposited films.

While the basic-setup is simple relative to many other deposition techniques, the physical phenomena of laser-target interaction and film growth are quite complex (see Process below). When the pulsed laser is absorbed by the target, energy is first converted to electronic excitation and then into thermal, chemical and mechanical energy which results in evaporation, ablation, plasma formation and even exfoliation [8]. The ejected species then expand into the surrounding vacuum in the form of a plume containing many energetic species including atoms, molecules, electrons, ions, clusters, particulates and molten globules, before depositing on the typically hot

substrate.

The history of laser-assisted film growth started soon after the technical realization of the first laser in 1960 by Maiman. Smith and Turner [9] utilized a ruby laser to deposit the first thin films in 1965, three years after Breech and Cross studied the laser-vaporization and excitation of atoms from solid surfaces. . However, the deposited films were still inferior to those obtained by other techniques such as chemical vapor deposition and molecular beam epitaxy. In the early 1980's, a few research groups (mainly in the former Union of Soviet Socialist Republics, USSR) achieved remarkable results on manufacturing of thin film structures utilizing laser technology. The breakthrough came in 1987 when Dijkkamp and Venkatesan were able to laser deposit a thin film of $YBa_2Cu_3O_7$, a high temperature superconductive material, which was of more superior quality than films deposited with alternative techniques. Since then, the technique of Pulsed Laser Deposition has been utilized to fabricate high quality crystalline films. The deposition of ceramic oxides, nitride films, metallic multilayers and various superlattices has been demonstrated. In the 1990's the development of new laser technology, such as lasers with high repetition rate and short pulse durations, made PLD a very competitive tool for the growth of thin, well defined films with complex stoichiometry.

Compared to other deposition techniques PLD has many advantages [10], which are listed as follow:

1) Good ability to fabricate thin film with very complex compositions from bulk materials;

2) Relatively high growth rate of about 1 – 5 Å per pulse;

3) Decoupled laser energy source from deposition environment;

4) No ultrahigh vacuum requirement;

5) Wide range of ambient reactive gas pressures (from 10-7 to 1 mbar);

6) Relatively simple fabrication setup for in-situ growth of different material with multilayer structure;

7) Reduced film contamination due to the use of light for promoting ablation.

However, PLD also has its limitations, such as:

1) Relative small deposition area;

2) Existence of large particulates that was ejected from the target.

However, deposition area can be increased to a certain extent by sweeping laser beam across target, while large particulates can be easily filtered by using a suitable spinning disc containing an aperture synchronized to the laser pulses.

In contrast to the relatively simple experimental setup for PLD, the theory of PLD mechanism is highly complex. Detailed explanations on the theory and mechanism of PLD can be found in references such as [11].

Figure 3.1 shows the diagram of a typical PLD system. We used a high energy KrF excimer laser (pulse duration 30 ns, wavelength 248 nm, Lambda Physik Lextra 200). The laser is first reflected by a mirror and then focused through a focusing lens outside the vacuum chamber. The target holder is customized such that it can hold up to 2 different targets inside the chamber. This would enable us to grow different thin film layers without breaking the vacuum by rotating the holder to the desired target

[12]. This would also help to keep the sample clean during the deposition. The target rotates around its axis during deposition to minimize the large particulate splashing effect and to achieve a more uniform ablation of the target. The distance between the target and the sample is around 4 cm. The chamber can be pumped down to a vacuum of around 1×10^{-6} mbar by a turbo molecular pump backed by a rotary pump.

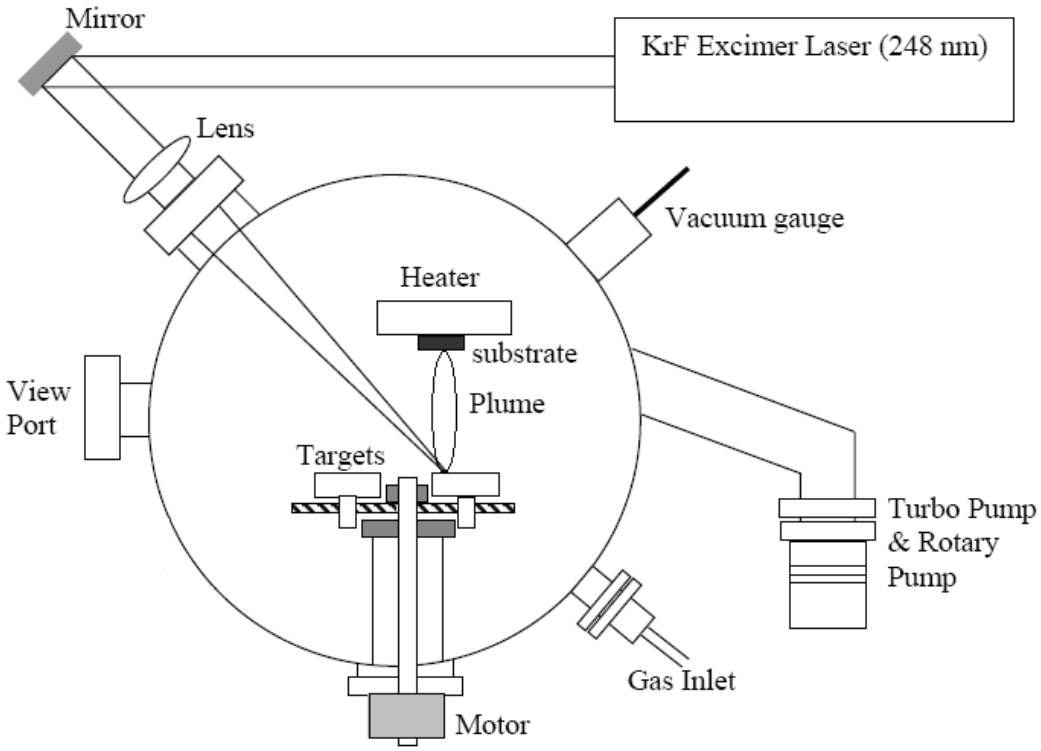

Figure 3.1 A schematic drawing of the pulsed laser deposition (PLD) system.

All the varactor thin film samples mentioned in this dissertation were deposited on commercial 0.5 mm thick, single-side polished LAO substrate (bought from Hefei Kejing Materials Technology Co. Ltd., Anhui, P.R.C) with <100> surface orientation. It is necessary for the substrate surface to be very clean prior to the deposition process to ensure fabrication of good quality thin film. The substrate was cleaned by first immersing it in an acetone (purity > 99.8 %) ultrasonic bath for 10 minutes to remove organic contaminants. Then it was flushed thoroughly with running distill water, and

immersed in a 10 % (by volume) nitric acid ultrasonic bath for 10 minutes to remove inorganic contaminants. The substrate was then again flushed thoroughly with running distill water, and immersed in acetone ultrasonic bath for 10 minutes. The substrate was then transferred to and stored in high purity ethanol (> 99.9 %) until it is ready to be loaded into the vacuum chamber. Before loading into the chamber, the substrate was blown dry using compressed nitrogen gas. The substrates were adhesively attached to sample holder (resistive heater) by applying a thin layer of silver paste.

As the BST thin films fabricated in this thesis were for the fabrication of microwave devices, the deposition parameters were optimized for the best crystal quality which was measured using the characterization method described in chapter 3. The BST thin films were deposited with the following optimized parameters: energy density of 2.5 J/cm2, target to substrate distance of 4.3 cm, temperature at 760°C and oxygen pressure at 0.2 mbar. The deposition time is 30 minutes with the laser pulse repetition rate at 3Hz. After deposition, the BST thin film was annealed at 700°C for 30 minutes at oxygen pressure of 1 bar. The detailed procedure of the thin film deposition process is listed in appendix 1.

3.2 Crystal and microstructure characterizations

In this section, the methods used to characterize the varactor thin film samples mentioned in this dissertation are reviewed.

3.2.1 X-ray diffractions

X-ray scattering techniques are a family of non-destructive analytical techniques which reveal information about the crystallographic structure, chemical composition,

and physical properties of materials and thin films [13]. These techniques are based on observing the scattered intensity of an x-ray beam hitting a sample as a function of incident and scattered angle, polarization, and wavelength or energy. Gonio (θ-2θ) scans were used to identify the crystalline phase and determine the out-of-plane crystal orientation of the deposited film. In Gonio scan, an x-ray beam was incident on sample at an angle of θ with respect to the surface of the sample. The x-ray was then diffracted by the crystal lattice of the samples. The intensity of the diffracted beam at an angle of 2θ with respect to the incident beam is measured to obtain the intensity versus θ or 2θ diffraction spectrum. Peaks can occur in the diffraction spectrum at values of θ where the Bragg's equation is satisfied, i.e.:

$$n\lambda = 2d\sin\theta, \qquad (3.1)$$

where n is an integer, λ is the X-ray wavelength and d is the distance between adjacent crystal planes with the same Miller index.

The XRD measurements presented in this dissertation were carried out using the Philips PW1710 based diffractometer controller (Philips Analytical X-ray, B. V., Almelo, Netherlands) at Department of Physics, National University of Singapore. The diffractometer used a PW2273/00 X-ray source with PW1729/40 high tension generator set at 30 kV and 20 mA to produced mainly copper $K_{\alpha 1}$ radiation (λ = 1.54056 Å) with a small amount of $K_{\alpha 2}$ radiation (λ = 1.54439 Å). The diffractometer used the PW1820 goniometer with PW1768 specimen holder. A PW1397/60 theta drive1 was mounted on the goniometer for rocking curve measurement. A PW1711/10 xenon filled proportional counter1 with a PW1752 graphite

monochromator1 was used to detect the diffracted X-ray. Control of the diffractometer and data collection/analysis was done using a personal computer running the PC-APD (PW1877) (Version 3.6B) XRD peak analysis software. Functions of the software include peak search, curve smoothing, $K_{\alpha 2}$ stripping and background subtraction. The θ-2θ scans were usually done using the following parameters: continuous scan mode from 10° to 70°, sampling time of 1 second per step and step size of 0.1°. The results were then compared to the standard powder diffraction file [14] and the publications in the open journals, for determination of the phase composition, crystal orientation and lattice parameters of the films deposited.

3.2.2 Scanning electron microscope and atomic force microscope

In order to investigate the morphology and microstructure of the ferroelectric films deposited, we employed scanning electron microscope (SEM) and atomic force microscope (AFM). Both SEM and AFM provide a convenient way to visualize the surface topography of BST and LSMO thin film, with no prior sample preparation required. While both SEM and AFM can be used to observe features such as defects, particulates and grain structure, SEM provides a rapid means of imaging both large and small surface area. Imaging with AFM is comparatively much slower and only a small section of the surface can be scanned at a time (maximum area of $90 \times 90\ \mu m^2$ for the instrument used here). The main advantage of AFM lies in its ability to provide quantitative height analysis such as surface roughness.

In SEM characterization, electrons are emitted from a very fine tungsten tip by applying a high voltage of several thousands of voltage to it. The electrons are then

focused through a series of magnetic lenses onto samples. The bombardment of the electrons will cause backscattered electrons and secondary electrons to be emitted from sample surface. These backscattered and secondary electrons are collected and analyzed. Since the backscattered and secondary electrons collected usually come from the surface of films, the image formed would normally reflect the surface morphology of samples observed.

SEM equipment used in this study is JSM-6700F field emission scanning electron microscope (Jeol, Tokyo, Japan). It is equipped with a field emission electron gun of 5 kV to 20 kV and a current of 5 mA to 20 mA, which can be adjusted depending on condition of the samples. Since ferroelectric materials are insulators, a very thin layer of gold or platinum was coated onto surface of the sample for better conduction of electrons before using SEM to image samples. The conductive coating prevents the build-up of electric charge on the sample to ensure the quality of SEM images.

We used AFM to characterize the average surface roughness and the grain size distribution of our thin films. AFM images of the LSMO thin films presented in this dissertation were taken using the Digital Instruments Dimension 3000 atomic force microscope (Veeco Instruments Inc., New York, USA) at Department of Physics, National University of Singapore.

AFM technique is also widely used to characterize surface morphology of thin samples [15]. In AFM characterization, a very sharp probe, in our case which is made of silicon nitride, is positioned on the surface of sample. A constant force is then maintained between the probe and the sample surface while the probe is scanned

across the sample surface. By monitoring the probe, a 3-dimensional image of the sample surface can be constructed. The constant force is maintained by measuring the level of the reflected laser from the probe with a “light lever” sensor. The signal is then fed into a feedback unit that controls the piezoelectric driver unit of the probe. The advantage of AFM over SEM is that the sample does not need to be conductive. However the resolution of the AFM highly depends on the surface roughness of the sample and the scanning areas of AFM are usually smaller compare to SEM.

There are two operation modes, contact and tapping mode that can be used for scanning the surface of samples. Contact mode means that the tip of probe is scanned at a near proximity of sample surface. The feedback systems of the AFM monitor the force between the tip and the sample and adjust the piezoelectric driving unit accordingly. The advantage of contact mode is that one can obtain a better contrast and closer morphology details of the sample surface. However since the tip is placed very close to the sample, there are possibilities for tip to pick up sample debris and to lose contact when the surface is too rough. In tapping mode, the tip is oscillated at a frequency near the resonance of the AFM probe. The tip is then placed at a much elevated position on top of the sample. The AFM feedback systems monitor the changes in the resonance frequency and adjust the position of the tip accordingly. The advantage of the tapping mode is that one can prevent any scratching of the sample and maintain contact with the sample even if the surface roughness is large.

3.2.3 Electrical and ferroelectric characterizations

The dielectric properties of the ferroelectric thin films were characterized using

an HP 4194A impedance analyzer [16] and HP 8722D Vector Network Analyzer (VNA). The measuring frequency range of impedance analyzer is from 1 kHz to 13 MHz while the frequency range of VNA is from 50MHz to 10GHz. The thin film samples were prepared with a capacitor sandwich structure. Ferroelectric films were deposited onto bottom electrodes of either metallic conductor such as platinum or conductive oxide such as LSMO. Au (gold) was then sputtered on top of the ferroelectric thin films as top electrodes.

By using HP 4194A impedance analyzer, a probe station was used for the electrical measurement of the samples. The probe station has two traveling manipulators which can be adjusted in x, y and z directions with microscrews. A tungsten tip is attached at the end of each manipulator to provide electrical contact to samples. An optical microscope is equipped above the probe station to provide a magnified view for the positioning of the tungsten probes onto samples.

By using HP 8722D VNA, a three-pin probe was used for measuring high frequency dielectric properties. The pin in the middle is connected to an electrode while the pins on both sides are connected to the other electrode. Also the optical microscope is equipped above the probe station to provide a magnified view for the alignment.

References

[1] S. Otsubo, T. Maeda, T. Minamikawa, Y. Yonezawa, A. Morimoto and T. Shimizu, "Preparation of $Pb(Zn_{0.52}Ti_{0.48})O_3$ Films by Laser Ablation", *Jpn. J. Appl. Phys. Part 2* **29** 133, (1990).

[2] H. Buhay, S. Sinharoy, W.H. Kanser, M.H. Francombe, D.R. Lampe and E. Stepkee, "Pulsed Laser Deposition and Ferroelectric Characterization of Bismuth Titanate Films", *Appl. Phys. Lett.* **58,** 1470 (1991).

[3] D. Roy, S. B. Krupanidhi and J. P. Dougherty, "Excimer Laser Ablated Lead Zirconate Titanate Thin Films", *J. Appl. Phys.* **69,** 7930 (1991).

[4] K. D. Budd, S. K. Dey and D. A. Payne, "Sol-Gel Processing of $PbTiO_3$, $PbZrO_3$, PZT AND PLZT Thin Films", *Br. Ceram. Proc.* **36**, 107 (1985).

[5] S. B. Majumder, D. C. Agrawal, Y. N. Mohapatra and V. N. Kulkarni, "Perovskite phase formation in sol-gel derived $Pb(Zr_xTi_{1-x})O_3$ thin films", *Int. Ferro.* **8**, 217 (1995).

[6] M. Ichiki, J. Akedo, A. Schoroth, R. Maeda, Y. Ishikawa, "X-Ray Diffraction and Scanning Electron Microscopy Observation of Lead Zirconate Titanate Thick Film Formed by Gas Deposition Method", *Jpn. J. Appl. Phys.* **36**, 5815 (1997).

[7] C. Lucat, F. Menil, and R. R Von Der Mühll, "Thick-film densification for pyroelectric sensors", *Mea. Sci. & Tech.* **8**, 38 (1997).

[8] Pulsed Laser Deposition of Thin Films, edited by Douglas B. Chrisey and Graham K. Hubler, John Wiley & Sons, 1994

[9] H. M. Smith and A. F. Turner, "Vacuum deposited thin films using a ruby laser", *Appl. Opt.* **4**, 147 (1965).

[10] S. Ghosh and P. Adler, "Competing magnetic interactions and large magnetoresistance effects in a layered iron (IV) oxide: citrate–gel synthesis and properties of $Sr_3Fe_{1.8}Co_{0.2}O_{\sim 7}$", *Solid State Comm.* **116**, 585 (2000).

[11] D. B. Chrisey and G. K. Hubler, "Pulsed Laser Deposition of Thin Films", John Wiley & Sons, 1994.

[12] S. Y. Xu, C. W. Tan and C. K. Ong, "Designs of multi-target carousels for pulsed-laser deposition systems", *Meas. Sci.& Tech.* **9**, 1912 (1998).

[13] B. D. Cullity and S. R. Stock, "Elements of X-Ray Diffraction", 3rd Ed., Prentice

Hall, 2001.

[14] Powder diffraction file: PDF-2 database (Computer file), International Center for Diffraction Data, 1996-2000

[15] K. D. Budd, S. K. Dey, and D. A. Payne, “Sol-Gel Processing of $PbTiO_3$, $PbZrO_3$, PZT AND PLZT Thin Films”, *Br. Ceram. Proc.* **36**, 107 (1985).

[16] HP 4194A Impedance Analyzer Operating Manual, Hewlett Packard (2000).

CHAPTER 4:

FABRICATION OF VARACTOR

In this chapter, we mainly concern about the thin film deposition and structure characterization including XRD, SEM and AFM pictures. Three varactors were fabricated, using LSMO, Pt and Au as their bottom electrode respectively. Deposition and characterization of LSMO and BST thin film are discussed in detail. Au deposition is listed in appendix 2 because it is relative simple.

4.1 Deposition of LSMO thin film

4.1.1 Procedures and parameters of LSMO thin film deposition

The brief introduction of PLD system and thin film deposition has already been presented in chapter 3. Detailed procedures of operating PLD are listed in appendix 1. In the present work, perovskite conductive oxides were chosen as bottom electrode besides conventional metal layer. Recently this issue has been extensively studied, and results of which have clearly shown the advantages in structure compatibility, chemical stability and fatigue-resisting property of conducting oxides like YBa_2CuO_7, (La, Sr)MnO_3 (LSMO), $LaNiO_3$ and $SrRuO_3$ [1-3]. The lattice of LSMO a=b=3.85 Å while the lattice of BST is a=b=3.947 Å. The PLD system employed in this experiment has been employed to fabricate various high qualities epitaxial thin films [4-9]. The target used was a sintered BST ceramic, which had a composition of Ba0.5Sr0.5TiO3. The target-to-substrate distance was 4.3 cm. The incident angle of the laser beam with respect to the target surface was 45 degree.

Polished (100) LAO single crystal substrate with a size of 5 mm × 10 mm × 0.5

mm was used as substrate. Before deposition, all LAO substrates were cleaned in acetone for 10 minute by ultrasonic vibration to remove residual oxide layer on the surface. A serious of temperatures were tested from 650°C to 750°C

The crystalline phases and orientation of the films were characterized using X-ray diffraction (XRD) θ-2θ scan. Ferroelectric thin film with identical composition but deposited under different deposition condition can have very different complex permittivity due to structural effects such as defects, mechanical stress, and interface and surface behaviors. During the experiment, the temperature factor affects the quality of LSMO thin film most. So the present work specially studies the effect of deposition temperature on the morphology of LSMO thin film surface by AFM operating under tapping mode.

4.1.2 Results and discussion

Figure 4.1 shows the XRD patterns of the LSMO film deposited for 30 minutes, where only high and sharp (001) and (002) peaks of LSMO and peaks of the LAO substrate are observed. The film was well crystallized and oriented, as revealed by XRD analysis. Referring to the Bragg's equation listed in chapter 3, $n\lambda = 2d\sin\theta$ and the lattice parameter of LSMO and LAO, 3.85 Å and 3.789 Å respectively, we can identify the angle of LSMO (00*l*) peak is smaller than that of LAO (00*l*) peak, where *l* is the integral index. For the same *n* and λ, $2d\sin\theta$ is kept as a constant. So if *d* is bigger, then the sinθ would be smaller. Then the θ would be smaller correspondingly. However, only the XRD graph is not sufficient to determine that quality of LSMO thin film is high enough to be used for the following growth of BST thin film. The

surface of LSMO is a key issue, too. Smooth surface will help BST thin film grows and crystallizes better.

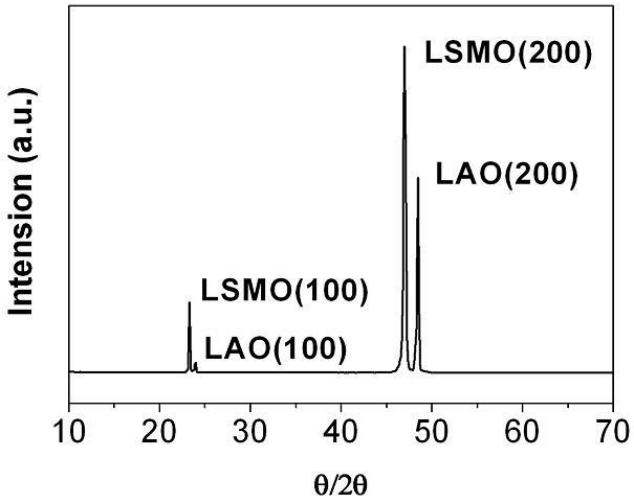

Figure 4.1 XRD θ/2θ scan of the LSMO film (900nm) deposited on (100)LAO substrate for 30 minutes at 750°C.

AFM and SEM facilities are used to study the surface morphology of LSMO. The effect of temperature was investigated. Three LSMO/LAO samples are fabricated in 650°C, 700°C and 750°C respectively. Figure 4.2 shows typical AFM micrographs of the films with different deposition temperature.

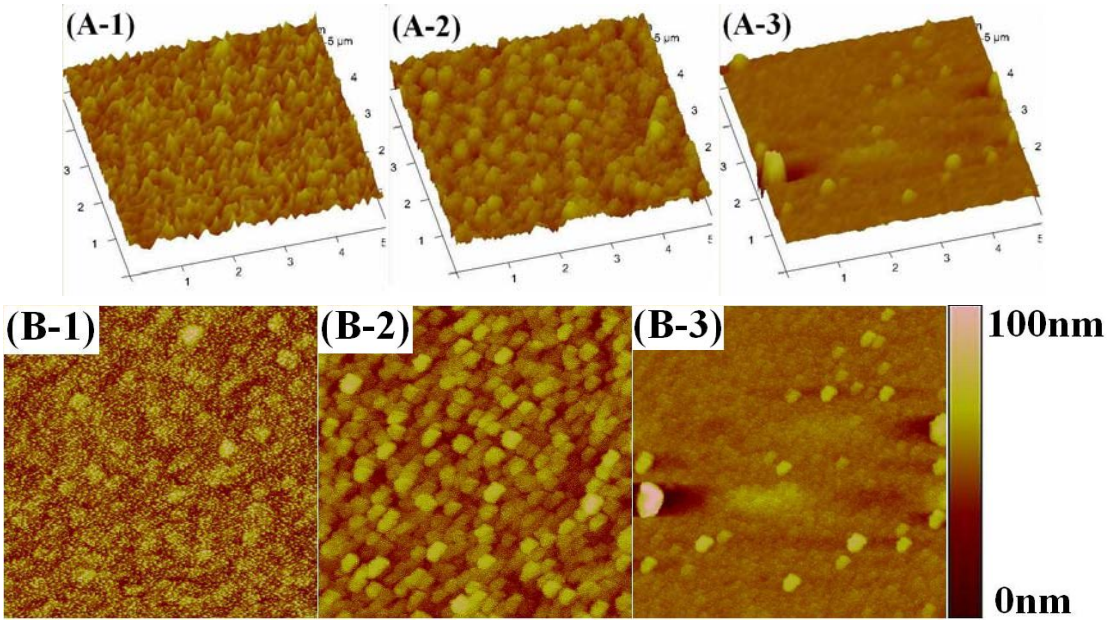

Figure 4.2 AFM pictures of surface morphology of LSMO at different temperature (A-1), (B-1) at 650°C; (A-2), (B-2) at 700°C and (A-3), (B-3) at 750°C. (A) are 3-D view pictures while (B) are top view pictures.

The average roughness (R_a) of each sample has been obtained by the controlling computer, listed in table 4.1.

Sample Name	LSMO-1	LSMO-2	LSMO-3
Average Roughness (R_a)	9.94nm	8.01nm	3.91nm

Table 4.1 Average roughness of LSMO thin film deposited in different temperature.

Clearly from Table 4.1, LSMO thin film deposited at 750°C is the smoothest thin film. As the temperature decreases, the roughness of the LSMO thin film increases and becomes more and more difficult to grow high quality BST thin film on it. High temperature would help improve lattice ordering. Since LSMO is forming columnar grains, size will be increased at higher temperature. Thus for the following fabrication of varactor, deposition temperature of 760°C for LSMO was chosen.

4.2 Deposition of BST thin film at the top of different bottom electrode

4.2.1 BST target preparation

The targets used in PLD are usually prepared using the solid-state reaction method. While a single-crystal target is better, as a high-density target reduces the particulates in the resulting thin film, single-crystal form of multi-components targets such as $Ba_{0.5}Sr_{0.5}TiO_3$ are usually not readily available or easily prepared. As such, solid-state reaction is the most commonly used synthesis method for preparing multi-components ceramic targets. The advantages of the solid-state reaction include the ready availability of oxide precursors, low cost and the precise weighting of the

reaction components.

Solid-state target preparation of oxide target involves the repeated grinding, compaction, and sintering of the component oxides until a pure phase material is achieved. A common variation of this technique is the use of carbonates or oxalates as precursors for the oxides. Upon the first calcining, the precursors decompose into ultra fine grain oxide powders. The high reactivity of these powders helps the solid-state reaction process in the following sintering. As the solid-state reaction method depends on the inter-diffusion between the oxide powders, it is necessary to use fine, well-compacted powders and to sinter them at a temperature high enough for the diffusion length to exceed the particle size.

The $Ba_{0.5}Sr_{0.5}TiO_3$ targets were prepared using solid-state reaction of $BaTiO_3$ and $SrTiO_3$ powders with particle size of less than 2 micron and purity greater than 99.9 %. The $BaTiO_3$ and $SrTiO_3$ powders with the composition molar ratio of 5:5 were mixed evenly together by ball milling. The mixed powder was then heated at 1250°C for 2 hours. The fired sample was ball milled again and the resulting powder is cold pressed into a disc shape target with a pressure of about 3000 kg/cm2 using a hydraulic press. The disc was then sintered in atmospheric environment with the following heating profile:

- Heat from room temperature to 650°C at 5°C /minute, then maintain at 650°C for 6 hours.
- Heat from 650°C to 1425°C at 5°C /minute, then maintain at 1425°C for 24 hours.
- Cool from 1425°C to 650°C at 5°C /minute, then maintain at 650°C for 6 hours.

- Cool from 650°C to room temperature at 5°C /minute.

4.2.2 Thin film deposition

Three BST parallel plate varactors using $La_{0.7}Sr_{0.3}MnO_3$ (LSMO), Pt and Au as bottom electrodes were fabricated to carry on the study. The XRD of the multi-layer thin films of the three varactors is shown in Figure 4.3. The (00*l*) BST thin film (400nm) was grown epitaxially on LSMO and Pt, as having been reported by many groups [10]. The crystal parameters of LSMO and Pt are 3.85 Å and close to BST, making epitaxial growth possible. However, the BST thin film on Au has (111) and (200) peaks and thus multi-oriented.

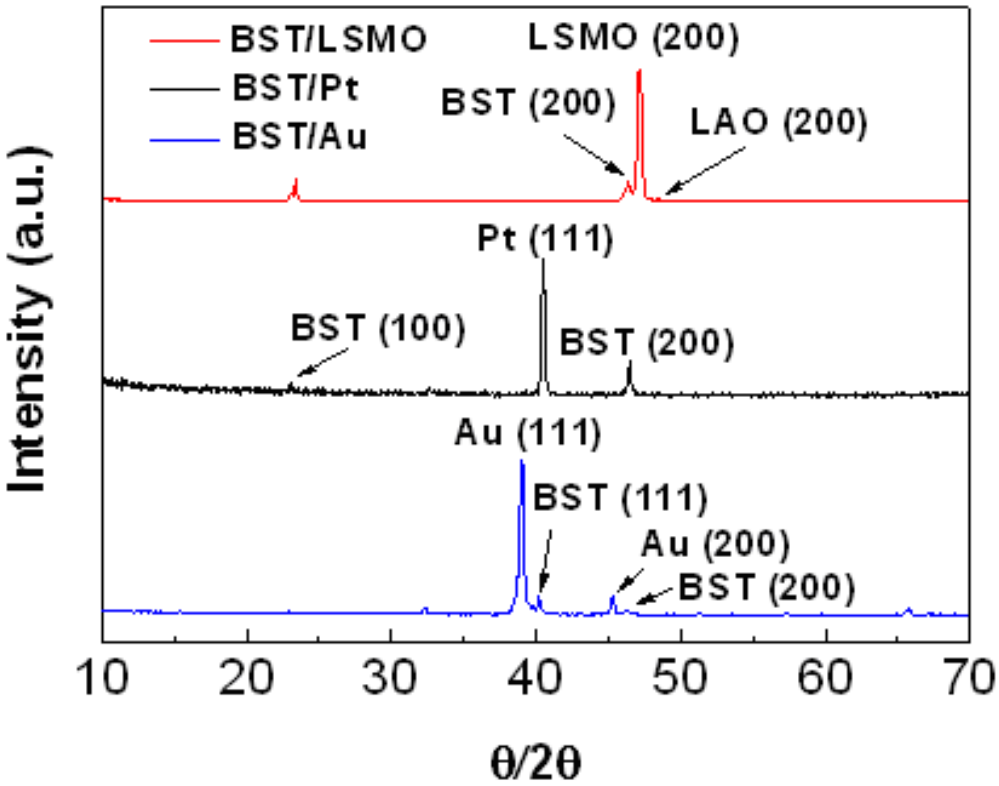

Figure 4.3 XRD of three varactors with different bottom electrodes, from top to bottom is BST/LSMO, BST/Pt and BST/Au.

SEM cross-section views of the three varactors are shown in Figure 4.4. Clearly, the epitaxial BST thin film on both LSMO and Pt shows columnar grains and clear interfaces. On the contrary, the interface between BST and Au shows some defects.

Many ferroelectric thin film properties are dependant on the quality of the grown film [11, 12]. The dielectric constant of BST in BST/Au varactor is smaller than in the other two varactors because polycrystalline BST thin film has more defects than epitaxial ones. The thickness of each layer was also obtained from these SEM pictures. The Au bottom layer in BST/Au varactor is about 2 μm, approaching the gold skin depth at 10 GHz. Thus the effect of skin depth to the resistance is reduced significantly.

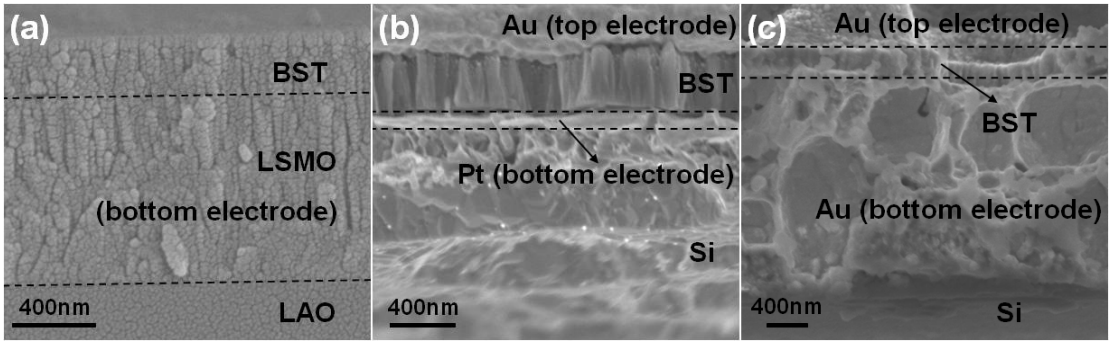

Figure 4.4 SEM cross-section view of (a) BST/LSMO (b) BST/Pt (c) BST/Au varactor.

Lithography and wet etching was used to pattern the top electrode. The detailed procedures are listed in appendix 3.

References

[1] J. F. Scott, C. A. Araujo, B. M. Melnick, L. D. Macmillan and R. Zuleeg, "Quantitative measurement of space-charge effects in lead zirconate-titanate memories", *J. Appl. Phys.* **70**, 382 (1991).

[2] R. Ramesh, W. K. Chan, B. Wilkens, T. Sands, J. M. Tarascon, V. G. keramidas, D. K. Fork, J. Lee and A. Safari, "Fatigue and retention in ferroelectric Y-Ba-Cu-O/Pb-Zr-Ti-O/Y-Ba-Cu-O heterostructures", *Appl. Phys. Lett.* **61**, 1537 (1992).

[3] D. J. Lichtenwalner, R. Dat, O. Auciello, and A. I. Kingon, "Effect of electrodes on the ferroelectric properties of pulsed-laser ablation-deposited $PbZr_XTi_{1-x}O_3$ thin film capacitors", *Ferroelectrics* **152**, 97 (1994).

[4] B. L. Low, S. Y. Xu, C. K. Ong, Z. X. Shen and X. B. Wang, "Substrate temperature dependence of the texture quality in YBCO thin films fabricated by on-axis pulsed-laser ablation", *Supercond. Sci. Tech.* **10,** 41 (1997).

[5] S. Y. Xu, B. L. Low, C. K. Ong and X. Zhang, "Fabrication of double-sided YBa2Cu3O7_x thin films by the off-axis pulsed-laser deposition", *J. Mater. Sci. Lett.* **16,** 429 (1997).

[6] J. M. Liu, and C. K. Ong, "The large magnetoresistance property of $La_{0.5}Sr_{0.5}CoO_{3-x}$ thin films prepared by pulsed laser deposition", *Appl. Phys. Lett.* **73**, 1047 (1998).

[7] Q. Huang, J. M. Liu, J. Li, H. C. Fang, H. P. Li and C. K. Ong, "Oxygen deficiency dependence of magnetic and magnetoresistive properties for $La_{0.5}Sr_{0.5}CoO_{3-x}$ thin films prepared by pulsed laser deposition", *Appl. Phys. A-Mater. Sci. & Proc.* **68,** 533 (1999).

[8] H. C. Fang, C. K. Ong, S. Y. Xu, K. L. Tan, S. L. Lim, Y. Li and J. M. Liu, "Epitaxy barium ferrite thin films on $LiTaO_3$ substrate", *J. Appl. Phys.* **86**, 2191 (1999).

[9] X. Y. Zhang, C. K. Ong, S. Y. Xu and H. C. Fang, "Observation of growth morphology in pulsed-laser deposited barium ferrite thin films", *Appl. Surf. Sci.* **143,** 323 (1999).

[10] X. Y. Qi, J. Miao, X. F. Duan and B. R. Zhao, "Microstructure of $La_{0.7}Sr_{0.3}MnO_3/Ba_{0.7}Sr_{0.3}TiO_3/La_{0.7}Sr_{0.3}MnO_3$ epitaxial films grown on (0 0 1) $SrTiO_3$ substrate", *J. of Crystal Growth* **277**, 218(2005).

[11] S. Razumov, A. Tumarkin, O. Buslov, M. Gaidukov, A. Gagarin, A. Ivanov, A. Kozyrev, Y. W. Song, and C. S. Park, “Electrical properties of magnetron sputtered thin $BaSrTiO_3$ films depending on deposition conditions”, *Integrated Ferroelectrics*, **39**, 367 (2001).

[12] A. B. Kozyrev, V. N. Keis, G. Koepf, R. Yandrofski, O. I. Soldatenkov, K. A. Dudin, and D. P. Dovgan, “Procedure of microwave investigations of ferroelectric films and tunable microwave devices based on ferroelectric films”, *Microelectronic Engineering*, **29**, 257 (1995).

CHAPTER 5:

DIELECTRIC PROPERTIES OF THREE DIFFERENT BOTTOM ELECTRODE VARACTOR IN MICROWAVE FREQUENCY

In ferroelectric varactors, common used structures are parallel plate structure electrode [1] and interdigital structure electrode [2, 3]. The former structure is for the measurement of out-of-plane dielectric properties while the latter one is for the in-plane dielectric properties. Comparing with the interdigital structure, the parallel plate structure needs much smaller applied bias to achieve a relatively high tunability. So the parallel plate structure was used to fabricate the varactor device.

In this chapter, the characterization of $Ba_{0.5}Sr_{0.5}TiO_3$ ferroelectric thin films and $Ba_{0.5}Sr_{0.5}TiO_3$/LSMO, $Ba_{0.5}Sr_{0.5}TiO_3$/Pt and $Ba_{0.5}Sr_{0.5}TiO_3$/Au ferroelectric varactors are described.

5.1 Dielectric constant under applied bias and microwave frequency

Many efforts have been made in the characterization of the dielectric properties of ferroelectric thin films at microwave frequencies, and the methods developed generally fall into planar-circuit methods such as in [5-7] and near-field scanning microwave microscope methods such as in [8-10]. Figure 1 presents the most common used structure capacitor [11]. The former two are sandwich structure because there is a conductive layer called bottom electrode between the ferroelectric material and substrate. The latter two are two layer structure capacitors without the bottom electrode.

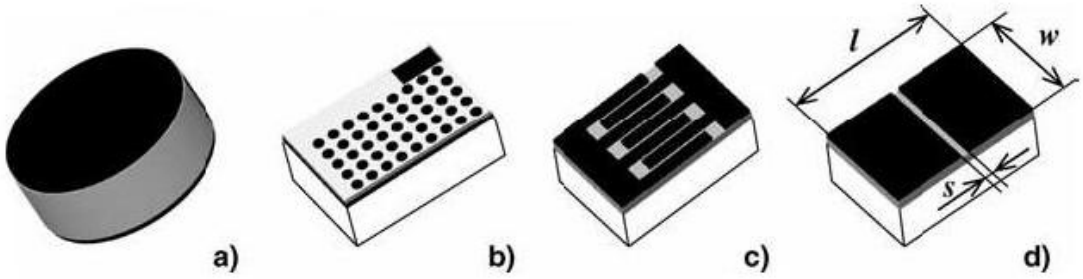

Figure 5.1 Different types of ferroelectric capacitors: (a) parallel plate capacitor, (b) array of parallel plate capacitors, (c) interdigital capacitor, (d) air gapped planar capacitor (in all pictures black color represents conducting electrodes, grey for ferroelectric material and white for substrate).

As mentioned at the beginning of this chapter, in the present work, a parallel plate structure was used to fabricate the varactor. Figure 2 shows a sketch of the cross-section view and top view of the whole varactor.

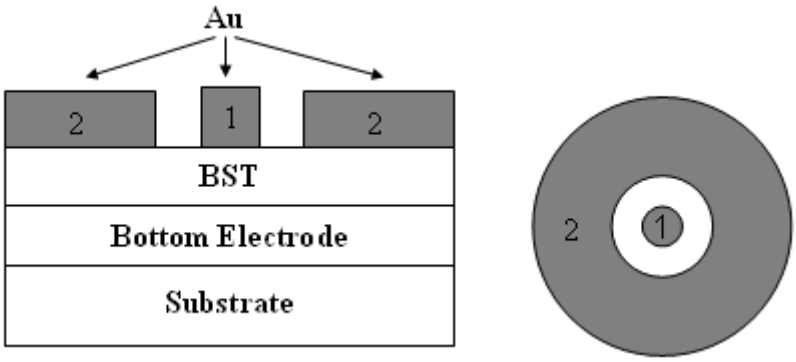

Figure 5.2 Cross-section (left) and top view (right) of the top electrode.

The pattern has a circle (marked as 1) at the center and a ring (marked as 2) around the circle. Comparing with other structure, the advantages of this circle pattern are (i) the outside ring may shield the electromagnetic noise. (ii) the electric field distribution in this pattern is regular and easy to calculate. (iii) it is easy to make high quality electrode with very small area. Two sizes of the pattern were used for different capacitance measurement apparatus. The big-size pattern is prepared for impedance analyzer because the signal from small sized electrode is comparable to the noise of impedance analyzer which renders the data to be indistinguishable from

the noise signal. The radius of the circle is 200 μm and the internal radius of the ring is 2000 μm with a 5000 μm external radius. On the other hand, the small-size pattern is designed for Vector Network Analyzer. The radius of the circle is 20 μm and the internal radius of the ring is 120 μm while the external radius of the ring is 500 μm. Microwave data was collected by HP 4194A impedance analyzer and HP8722D VNA with 3-pins measuring probe brought from GGB Industries, Inc. Figure 5.3 is a photograph of 3-pins probe on an X-Y-Z stage. The 3-pins probe simplifies the preparation steps for VNA measurement. The calibration is pinpointed right to the interface between top electrode of varactor and the three pins.

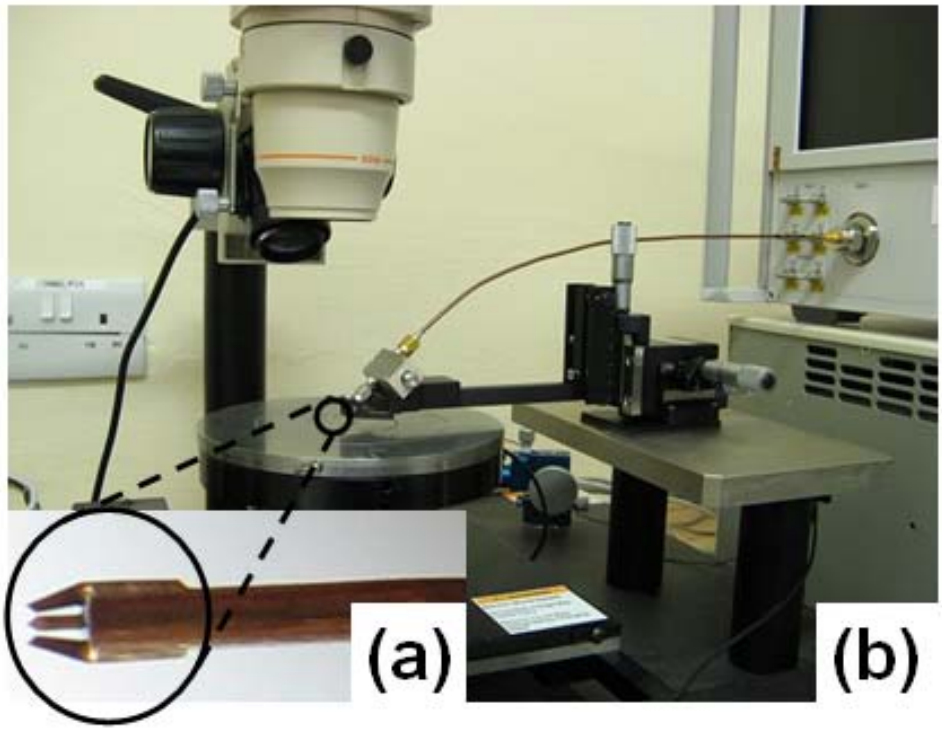

Figure 5.3 Photograph of 3-spins system (a) magnified image of 3-pins probe (b) whole X-Y-Z stage.

The dielectric constant and loss versus applied bias curve of BST/LSMO structure was measured by impedance analyzer at 0.1 MHz, shown as Figure 5.4. The dielectric constant at zero bias and 0.1 MHz is about 220 and the tunability is

50%. Comparing with the results from VNA presented as Figure 5.5, which shows a dielectric constant of 250 at zero bias and 200 MHz and a tunability of 52%, the data using big-size electrode pattern from impedance analyzer at 0.1 MHz is consistent with the data from VNA at 200 MHz. The small difference could be due to the experiment error.

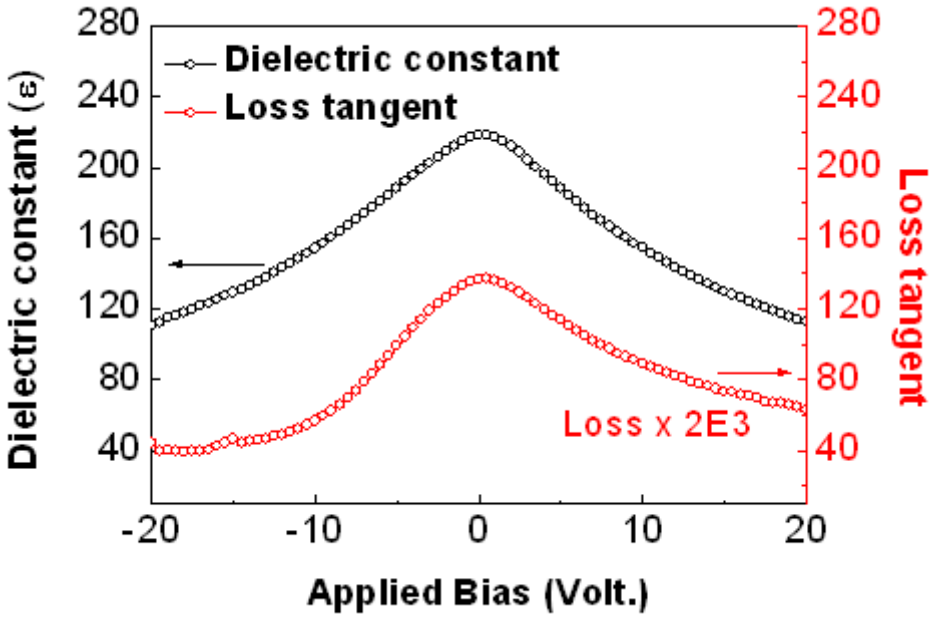

Figure 5.4 The dielectric constant and loss versus applied bias curve of BST/LSMO varactor.

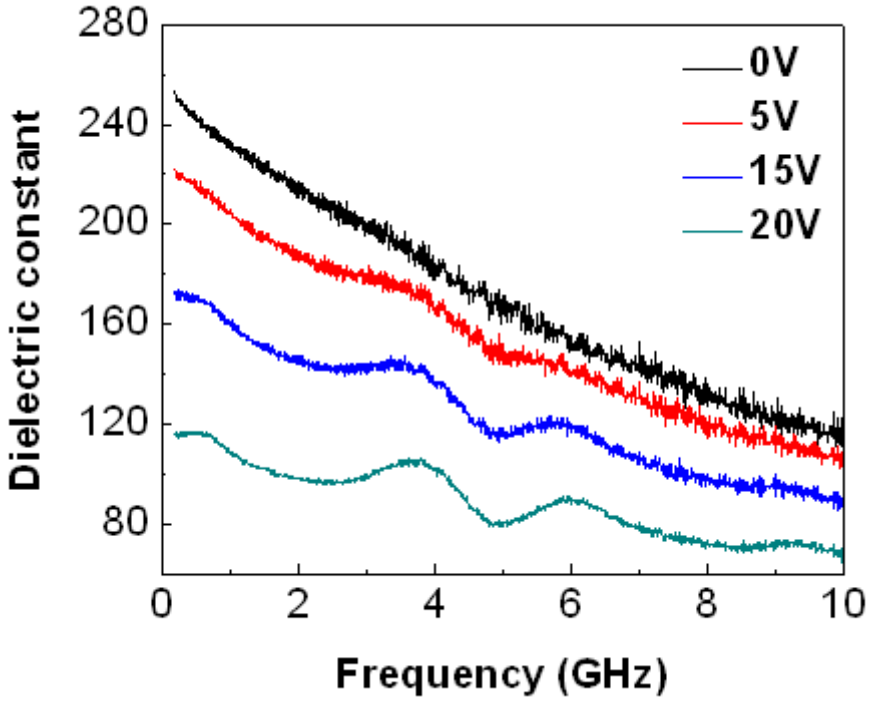

Figure 5.5 The dielectric dispersion on frequency of BST/LSMO varactor under different bias.

There is a significant reduction of dielectric constant while increasing the frequency. In theory however, the dielectric constant should be independent of frequency. The reason will be discussed below.

Before we start the discussion, we compare the frequency dependence of dielectric constant of the three structures in Figure 5.6. The dielectric constant of BST thin film from BST/LSMO and BST/Pt varactor is almost the same while that from BST/Au varactor is a little bit smaller at 200 MHz. This is due to the difference of crystal quality of BST on different bottom electrodes, as having been revealed by XRD and SEM results.

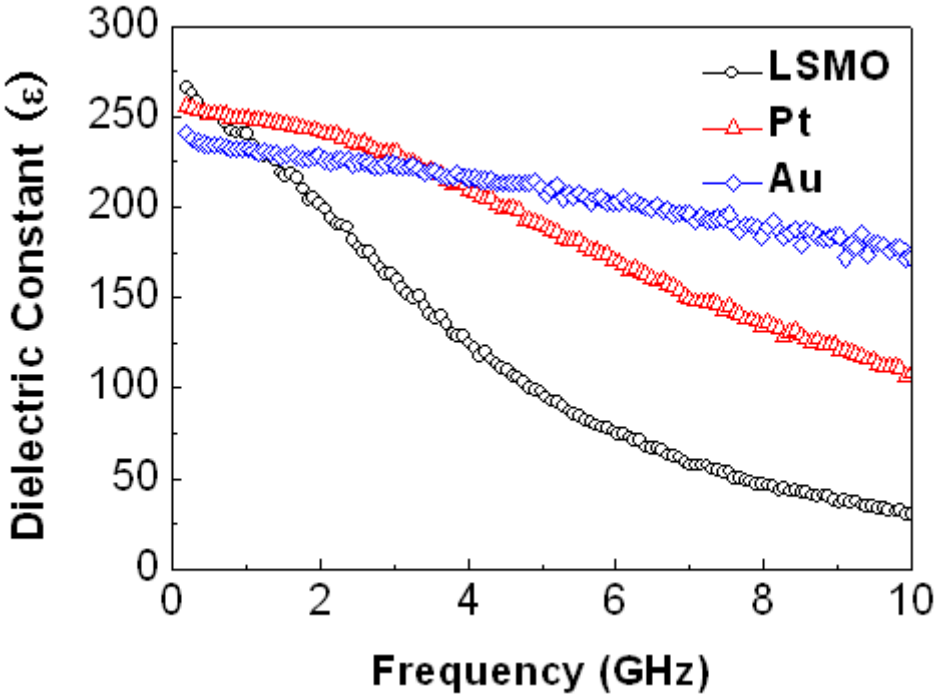

Figure 5.6 Dielectric constant versus frequency based on different bottom electrodes under zero bias. Black color presents BST/LSMO varactor, red color for BST/Pt varactor and blue color for BST/Au varactor.

In the figure 6, there is an obvious dielectric dispersion [12] as a function of frequency for all the three varactors. In the frequency range from 200MHz to 10GHz, BST/Au varactor's dielectric constant reduces the most slightly, only from 240 to 170, followed by BST/Pt varactor. BST/LSMO varactor reduces the most heavily. Then Origin program was used to fit the impedance versus frequency curve by using the equation $Z \approx R + \frac{1}{j\omega C_1}$ in order to pick out the resistance of the bottom electrode. The detailed derivatives of the equation are listed in appendix 4. The values of the three different bottom electrodes are listed in Table 5.1. The resistance of Pt and Au electrode is one order of magnitude lower than that of LSMO, with Au bottom electrode the lowest among these three.

Bottom electrode	Resistance (Ω)
LSMO	5.61 ± 0.029
Pt	0.96 ± 0.0082
Au	0.33 ± 0.0072

Table 5.1 Resistance of different electrodes of three varactors.

The behavior of dielectric constant versus frequency is different base on different bottom electrode. In the case that the bottom electrode is a perfect conductor, there is no voltage decrease along the length of bottom conductor. A sketch of the electric field distribution inside the varactor is shown on Figure 5.7 a). For the case of a varactor with electrode having lost mechanism, the electric field across the electrode become slanted (see Figure 5.7 b) due to the variation of voltage distribution across the bottom electrode. As a result, the effective d would become longer.

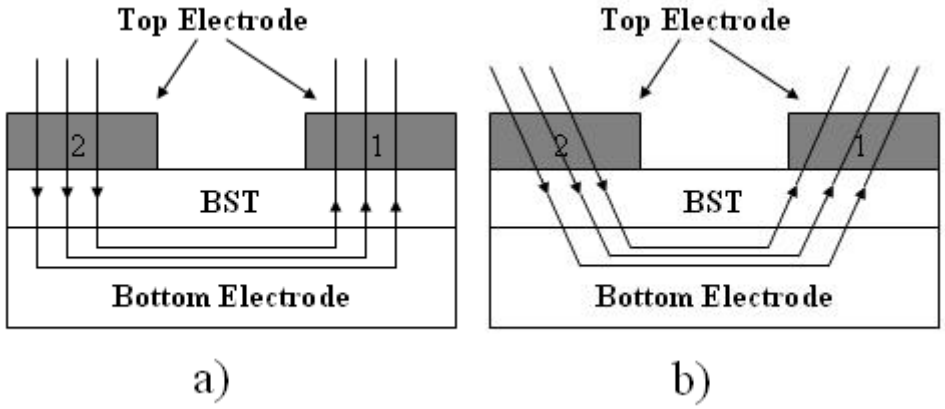

Figure 5.7 Electric field distributions in a) ideal situation b) real situation.

5.2 Loss tangent under microwave frequency

Normally, the loss factor in the bottom electrode would increase as the applied frequency increased. The effective d would consequently be increased as the

frequency increases. In the measurement of varactors, we normally take the separation of the electrodes as a constant value d_0. Therefore the frequency dependant formula for $C(f)$ becomes $C(f) = \varepsilon_0 \varepsilon_{eff}(f) \frac{A}{d_0}$. In conclusion, the better the conductor, the lesser the dependent of dielectric constant on frequency. There is also an undulation in the dielectric constant under an applied bias. This is due to the acoustic resonance reported in Ref. 13.

The loss of varactors with different bottom electrode was plotted in Figure 5.8. The loss of BST/LSMO varactor is very large, starting to beyond 1 at around 4 GHz. However, both BST/Pt and BST/Au varactor control their loss at small value and minimum loss of BST/Au is 0.014, measured at 0.2 GHz. It is close to the result reported by Prof. York group of the BZN/Au varactor's loss which is around 0.008 at 0.1 GHz. The maximum loss of BST/Au is 0.146 while it is 3.11 of BST/LSMO varactor measured at 10 GHz. Comparing with BST/LSMO varactor, BST/Au varactor's loss is reduced significantly due to its remarkably reduced bottom electrode resistance, already shown in Table 5.1.

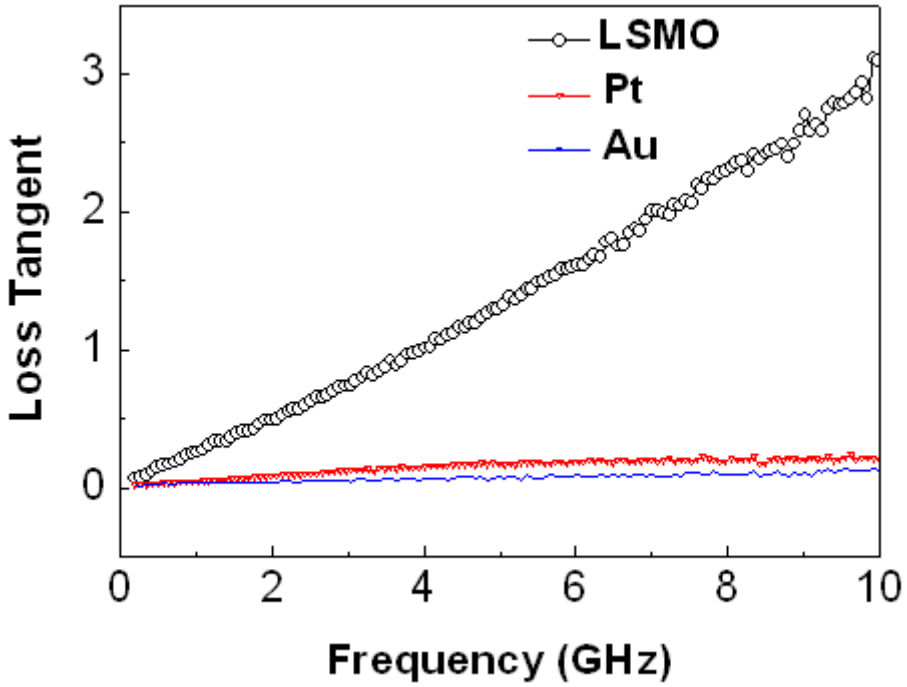

Figure 5.8 Loss versus frequency based on different bottom electrodes with zero bias.

The loss tangent can be expressed as tanδ=ωCR. From this equation, there are two ways to reduce the loss tangent: either by decreasing the capacitance or by decreasing the resistance of the bottom electrode. Because the capacitance of parallel plate capacitor is $C = \frac{\varepsilon_0 \varepsilon A}{d}$, ε_0 is a constant, can not be changed; the thickness d is not a good choice because it is nonlinearly related to capacitance. The contribution of thickness d to the capacitance reducing becomes smaller and smaller while increasing the thickness. Meanwhile, electrode area A is difficult to be shrunk infinitely because of technical issues. Thus one reasonable way to reduce the capacitance is trying to reduce the resistance of bottom electrode. This conclusion consists with the result of Figure 5.8.

References

[1] S. Gevorgian, T. Martinsson, P. L. J. Linner, and E. L. Kollberg, “CAD models for multilayered substrate interdigital capacitors”, *IEEE Trans. Microw. Theory Tech.* **44**, 896 (1996);

[2] A. Vorobiev, P. Rundqvist, K. Khamchane, and S. Gevorgian, “Silicon substrate integrated high Q-factor parallel-plate ferroelectric varactors for microwave/millimeterwave applications”, *Appl. Phys. Lett.* **83**, 3144 (2003).

[3] C. Y. Tan, L. F. Chen, K. B. Chong, and C. K. Ong, “Nondestructive microwave permittivity characterization of ferroelectric thin film using microstrip dual resonator”, *Rev. Sci. Instrum.* **75**, 136 (2004).

[5] A. B. Kozyrev, O. I. Soldatenkov, T. B. Samoilova, A. V. Ivanov, C. H. Mueller, T. V. Rivkin, and G. A. Koepf, “Response time and power handling capability of tunable microwave devices using ferroelectric films”, *Integrated Ferroelectrics* **22**, 849 (1998).

[6] D. Galt, J. C. Price, J. A. Beall, and T. E. Harvey, “Ferroelectric Thin-Film Characterization Using Superconducting Microstrip Resonators”, *IEEE Transactions on Applied Superconductivity* **5**, 2575 (1995).

[7] R. A. Chakalov, Z. G. Ivanov, Y. A. Boikov, P. Larsson, E. Carlsson, S. Gevorgian, and T. Claeson, “Fabrication and investigation of $YBa_2Cu_3O_{7-\delta}/Ba_{0.05}Sr_{0.95}TiO_3$ thin film structures for voltage tunable devices”, *Physica C* **308**, 279 (1998).

[8] D. E. Steinhauer, C. P. Vlahacos, F. C. Wellstood, S. M. Anlage, C. Canedy, R. Ramesh, A. Stanishevsky, and J. Melngailis, “Quantitative imaging of dielectric permittivity and tunability with a near-field scanning microwave microscope”, *Review of Scientific Instruments* **71**, 2751 (2000).

[9] J. H. Lee, S. Hyun, and K. Char, “Quantitative analysis of scanning microwave microscopy on dielectric thin film by finite element calculation”, *Review of Scientific Instruments* **72**, 1425 (2001).

[10] Y. Lu, T. Wei, F. Duewer, Y. Lu, N. B. Ming, P. G. Schultz, and X. D. Xiang, “Nondestructive Imaging of a Dielectric-Constant Profiles and Ferroelectric Domains with a Scanning-Tip Microwave Near-Field Microscope”, *Science*, **276**, 2004 (1997).

[11] A. K. Tagantsev, V.O. Sherman, K. F. Astafiev, J. Venkatesh and N. Setter, “Ferroelectric Materials for Microwave Tunable Applications”, *J. of Electroceramics*,

11, 5 (2003).

[12] M. S. Tsai, T. Y. Tseng, "Effect of bottom electrodes on dielectric relaxation and defect analysis of $(Ba_{0.47}Sr_{0.53})TiO_3$ thin film capacitors", *Materials Chemistry and Physics* **57**, 47 (1998).

[13] Deleniv, A., Sherman, V., Filhol, P. and Gevorgian, S., Workshop, "Parallel-plate waveguide bulk ceramic ferroelectric phase shifters", *2005 European Microwave Conference* **1**, 3 (2005).

CHAPTER 6:

CONCLUSION ON VARACTORS STUDY

In this thesis, the fabrication and characterization of three kinds of ferroelectric varactors BST/LSMO, BST/Pt and BST/Au were studied.

The introductory applications of chapter 1 gave a brief review on ferroelectric microwave applications. Chapter 2 reveals the theory and previous work that has been done by other research groups. Chapter 3 described the PLD technique and the fabrication procedures used to produce the LSMO and BST thin films. Also the principle of characterization facilities such as XRD, SEM and AFM are introduced. Chapter 4 reviewed the characteristics of thin film structure and surface morphology. In chapter 5, the dielectric properties of the three varactors were examined.

In the whole study, three parallel plate varactors with different bottom electrodes are fabricated using BST as the dielectric. The BST thin films are crystallized to have good tunability. The dependence of dielectric constant on frequency is explained by the electric field distortion due to the resistance of bottom electrode. Equation of loss related to the frequency, capacitance and electrode resistance was derived. The results of the varactor loss versus frequency demonstrate that the resistance of bottom electrode plays an important role in performance of the varactor in high frequency range. I hope that this study could provide some useful information of varactor performance in microwave application. The contribution of bottom electrode to the dielectric properties of varactor may help improve the design of microwave devices with better dielectric constant and lower loss.

The following major conclusions have been drawn from the results on the ferroelectric varactors in this thesis:

1. Not only perovskite metal oxide material is the candidate for being the bottom electrode of BST ferroelectric varactor, but Pt is suitable for high quality BST thin film growth.
2. The temperature affects the surface morphology of LSMO. Higher the temperature, smoother the surface of LSMO thin film grown.
3. The dielectric constant dependence on frequency is due to the electric field distortion which results in a longer separation of the electrodes. To reduce the dependence of the dielectric constant on frequency, the resistance of bottom electrode must be reduced.
4. The loss tangent is determined by the resistance of bottom electrode at high frequency. The study of ferroelectric varactors using the patterned top electrode, BST thin film and three different bottom electrode material including LSMO, Pt and Au are consistent with theory.
5. BST-Au varactor has the lowest loss and is the liveliest candidate for practical application.

List of publications by author

1. Magnetoelectric effect in epitaxial $Pb(Zr_{0.52}Ti_{0.48})O_3/La_{0.7}Sr_{0.3}MnO_3$ composite thin film, Ma, Y.G.; Cheng, W.N.; Ning, M.; Ong, C.K. **Source:** *Applied Physics Letters*, v 90, n 15, 2007, p 152911

2. Planar tunable high-temperature superconductor microwave broadband phase shifter with patterned ferroelectric thin film, Wang, P.; Tan, C.Y.; Ma, Y.G.; Cheng, W.N.; Ong, C.K. **Source:** *Superconductor Science and Technology*, v 20, n 1, Jan 1, 2007, p 77-80

APPENDIX 1:

PROCEDURE FOR PULSED LASER DEPOSITION OF BST THIN FILM

Precautions:

• Turn on the "Laser in operation" warning light and wear the laser safety goggles whenever the laser is turned on. Do not operate the laser when there are people not wearing laser safety goggles in the room.

• Wear clean powder-free latex or PVC gloves when handling anything in or will be going into the vacuum chamber. This is to avoid out-gassing from fingerprints.

1. Open the valve on the oxygen cylinder and set the regulator output pressure at 2 bar.
2. Switch on the vacuum gauge.
3. If the chamber had been previously pumped down, vent the vacuum chamber by opening the variable leak valve for the oxygen input. Fully close the variable leak valve when pressure within the chamber and the surrounding has equalized.
4. Open the vacuum chamber and load the cleaned substrates onto the heater with a pair of tweezers. Paste the substrate with a thin layer of silver paste on the substrate hold (heater). Turn on the temperature controller and heater power controller. Set the temperature controller to ramp up the temperature of the heater to 100°C. Maintain for 10 minutes to dry the silver paste then turn off the temperature controller and heater power controller
5. Close the chamber and fully open the gate valve.

6. Switch on the rotary vane pump.
7. When the pressure in the chamber is less than 0.1 mbar, switch on the turbo molecular pump and turn on the cooling water.
8. When the pressure of the chamber is less than 1×10^{-5} mbar, turn on the temperature controller and heater power controller. Set the temperature controller to ramp up the temperature of the heater to 760°C.
9. Half close the gate valve. Open and adjust the variable leak valve so that oxygen pressure is at 0.2 mbar.
10. Turn on the laser. The laser will take about 8 minutes to warm up before operation is possible.
11. When the temperature is at 760°C, turn on the motor driving the rotation of the BST target.
12. Set the laser to constant energy mode with per pulse energy of 230 mJ and pulse repetition rate of 3 Hz.
13. Deposition duration of 30 minutes is required when fabricating BST thin film with thickness of 400 nm.
14. At the end of the deposition period, stop the laser and the motor driving the target rotation.
15. Set the temperature controller to ramp down to 700°C
16. When the temperature is at 700°C, fully close the gate valve and open the variable leak valve to increase oxygen pressure to 1 bar. When the pressure is at 1 bar, shut off the variable leak valve.

17. Turn off the turbo molecular pump. Wait until the turbo molecular pump has automatically vented before turning off the rotary vacuum pump.
18. Anneal the BST thin film at 700°C and oxygen pressure of 1 bar for 30 minutes.
19. After annealing for 30 minutes, set the temperature to decrease to room temperature.
20. When the temperature has dropped to room temperature, turn off the oxygen cylinder valve and cooling water.
21. The substrate can now be taken out from the chamber.
22. Turn off the laser.
23. Open the gate valve and pump down the vacuum chamber to less than 1 mbar using the rotary vane pump. When pressure of less than 1 mbar is attained, closed the gate valve and turn off the rotary vane pump.
24. Turn off the vacuum gauge.

APPENDIX 2:

PROCEDURE FOR DEPOSITION OF GOLD FILM

1. Clean the substrate by one minute immersion in acetone ultrasonic bath, followed by one minute immersion in high purity ethanol ultrasonic bath. Blow dried the substrate with compressed nitrogen gas immediately upon removal from ethanol.
2. Visually inspect the surface of the substrate for the presence of particles e.g. dusts. If any particle is present, use compressed nitrogen gas to blow it off the substrate.
3. Place and align the substrate on the copper aperture mask.
4. Carefully load mask and substrate into the vacuum chamber of the ion sputtering unit (JFC-1100 Jeol, Tokyo, Japan) and inspect the alignment of the mask. If the alignment is correct, replace the bell jar of the vacuum chamber.
5. Set the controls of the sputtering unit to the following: power at off, HV switch at off, HV control at 0 and Vacuum control at 10.
6. Switch on the power.
7. Allow the vacuum chamber to pump down for 5 minutes.
8. Set the HV switch to DC. Gradually turn the HV control knob clockwise until the voltmeter indicates a reading of 500 V. If the ammeter reading is less than 2 mA, continue to step 9. If the ammeter reading is 2 mA or more, the vacuum is too low. Set the voltage back to 0 V and turn off the HV switch. Continue pumping for a longer period before repeating step 8.
9. Rotate the vacuum knob and HV control knob clockwise until the ammeter and the voltmeter indicates 10 mA and 1200 V respectively.

10. Allow the deposition to continue for nine minutes to obtain gold film of about 100 nm thick.
11. After nine minutes, turn the HV control knob to 0 and turn the HV switch to off.
12. Turn off the power and turn the vacuum knob fully clockwise to vent the vacuum chamber.
13. When pressure in the chamber has equalized, the bell jar can be removed and the gold coated substrate can be retrieved.

APPENDIX 3:

PROCEDURE FOR PHOTOLITHOGRAPHY AND WET ETCHING OF SUBSTRATE WITH GOLD TOP ELECTRODE

The following procedure is carried out in a darkroom with no UV light source such as white fluorescent lamp.

1. Clean the substrate by one minute immersion in acetone ultrasonic bath followed by one minute immersion in high purity ethanol ultrasonic bath. Blow dried the substrate with compressed nitrogen gas immediately upon removal from ethanol.
2. Load the substrate onto the spin coater (P6204, Specialty Coating System Inc., Indiana, USA).
3. Visually inspect the surface of the substrate for the presence of particles e.g. dusts. If any particle is present, use compressed nitrogen gas to blow it off the substrate.
4. Apply a few drops of photoresist (S1813, Shipley Co. Inc., Massachusetts, USA) onto the substrate. The photoresist should nearly cover the substrate surface but not overflow the edge. Spin the substrate at 6000 RPM for 60 seconds.
5. Remove the photoresist coated substrate from the spin coater and bake dry the photoresist at 120 °C for 5 minutes in a preheated oven.
6. Coat the second side of the substrate with photoresist by flipping the substrate over and repeating steps 2 to 5.
7. Load the substrate onto the mask aligner (Q-2001CT, Quintel Corp., California, USA). Use the microscope on the mask aligner to check for the presence of

defects like voids, bubbles or particles on the photoresist layer. If the photoresist layer contains any defect near or within the boundary of the region with device pattern, rinse off the photoresist with running acetone and repeat the procedure from step 1.

8. Load the soft mask onto the mask aligner. The printed side of the mask should be in contact with the photoresist. Check for the presence of particles on the mask by using the microscope on the mask aligner. If there is any particle, blow it off with compressed nitrogen gas.
9. Align the mask and substrate.
10. When the mask and substrate are aligned and in contact, expose the photoresist to UV light for 24 seconds. The UV light source on the mask aligner should be set to an output power of 250 W (note that the UV lamp should be allowed to warm up for at least 7 minutes before exposure to obtain the required intensity).
11. Remove the substrate from the mask aligner. Immerse the substrate in the photoresist developer solution (Microposit developer, Shipley Co. Inc., Massachusetts, USA) for 30 seconds to remove the exposed photoresist.
12. Thoroughly rinse the substrate with distilled water.
13. Remove the edge bead (if any) by wiping with a fine cotton swab soaked with acetone.
14. Etch away the unwanted region of the gold film by immersing the substrate into a KI (10 g), I_2 (5 g) and H_2O (500g) mixture for 20 seconds.
15. Thoroughly rinse the substrate with distilled water.

APPENDIX 4:

DERIVATIVE OF RESISTANCE OF BOTTOM ELECTRODE

Relation Between load impedance and reflection coefficient is

$$\Gamma = \frac{Z_L - Z_0}{Z_L + Z_0} \qquad (1)$$

where Γ is a complex number

Then equation (1) can be written like

$$Z_L = Z_0 \frac{1+\Gamma}{1-\Gamma} \qquad (2)$$

On the other hand, the impedance of whole varactor device is equal to

$$Z_L = R + \frac{1}{j\omega C_1} + \frac{1}{j\omega C_2} \qquad (3)$$

Referring to series capacitor model $\frac{1}{C} = \frac{1}{C_1} + \frac{1}{C_2}$, the total capacitance measured between two top electrodes is $C = \frac{C_1 C_2}{C_1 + C_2}$. Because C_2 is much larger than C_1, as we designed, C is approximately equal to C_1. The input impedance can be approximately written like that

$$Z_L \approx R + \frac{1}{j\omega C_1} \qquad (4)$$

C is a complex number which is $C = C' - jC''$ (5)

Substitute equation (5) into (4), get

$$Z_L = R + \frac{C''}{\omega(C'^2 + C''^2)} - j\frac{C'}{\omega(C'^2 + C''^2)} \qquad (6)$$

Equation (2) and (6) is equal, thus we can get real part of capacitance.

For a parallel plate capacitor, the capacitance is determined by following equation

$$C = \frac{\varepsilon_0 \varepsilon A}{d} \qquad (7)$$

So the dielectric constant is

$$\varepsilon = \frac{Cd}{\varepsilon_0 A} \qquad (8)$$

Substitute the C' into equation (8) we can get the ferroelectric material's dielectric constant

To get the resistance of bottom electrode, we use Origin program's curve fitting function. Set up a function using the real part of equation (6), which is

$$Z_{Lreal} = R + \frac{C''}{\omega(C'^2 + C''^2)} \qquad (9)$$

We have data of independent variable ω and coordinate variable Z_{Lreal}, so that we can get out the parameter R. The results are list below:

Bottom electrode	Resistance (Ω)
LSMO	5.61
Pt	0.96
Au	0.33